Received: 1 June 2024 | Revised: 1 October 2024 | Accepted: 21 October 2024

DOI: 10.1002/alz.14403

Alzheimer's & Dementia®
THE JOURNAL OF THE ALZHEIMER'S ASSOCIATION

RESEARCH ARTICLE

The tau isoform 1N4R confers vulnerability of *MAPT* knockout human iPSC-derived neurons to amyloid beta and phosphorylated tau-induced neuronal dysfunction

Sarah Buchholz[1,2] | **Mohamed Aghyad Al Kabbani**[1,2] | **Michael Bell-Simons**[1,2] | **Lena Kluge**[1,2] | **Cagla Cagmak**[1,2] | **Jennifer Klimek**[1,2] | **Natja Haag**[3] | **Lukas C. Iohan**[4,5] | **Audrey Coulon**[4] | **Marcos R. Costa**[4,6] | **Devrim Kilinc**[4] | **Hans Zempel**[1,2]

[1]Institute of Human Genetics, Faculty of Medicine and University Hospital Cologne, University of Cologne, Cologne, Germany

[2]Center for Molecular Medicine Cologne (CMMC), University of Cologne, Cologne, Germany

[3]Institute for Human Genetics and Genomic Medicine, Medical Faculty, RWTH Aachen University, Aachen, Germany

[4]Université de Lille, Inserm, CHU Lille, Institut Pasteur de Lille, U1167-RID-AGE- Risk factors and molecular determinants of aging-related diseases, Lille, France

[5]Bioinformatics Multidisciplinary Environment (BIoME), Federal University of Rio Grande do Norte, Campus Universitário, Lagoa Nova, Natal, Brazil

[6]Brain Institute, Federal University of Rio Grande do Norte, Campus Universitário, Lagoa Nova, Natal, Brazil

Correspondence
Hans Zempel, Institute of Human Genetics, Faculty of Medicine and University Hospital Cologne, University of Cologne, Kerpener Str. 34, 50931 Cologne, Germany.
Email: hans.zempel@uk-koeln.de

Funding information
Jürgen Manchot Stiftung; Koeln Fortune, Medizinische Fakultät, Universität zu Köln; Else Kröner-Fresenius-Stiftung; Deutsche Forschungsgemeinschaft; Studienstiftung des Deutschen Volkes

Abstract

INTRODUCTION: Human tau protein, composed of six brain-specific isoforms, is a major driver of Alzheimer's disease (AD). The role of its isoforms however remains unclear and human AD models are scarce.

METHODS: We generated human *MAPT*– (tau–) knockout (KO) induced pluripotent stem cells (iPSC) using CRISPR/Cas9, differentiated these into glutamatergic neurons, and assessed isoform-specific functions of tau in these neurons. We used omic- approaches, live-cell imaging, subcompartmental analysis, and lentivirus-based reintroduction of specific tau isoforms to investigate isoform-mediated neuronal dysfunction in an AD model.

RESULTS: Tau KO human iPSC-derived neurons showed decreased neurite outgrowth and axon initial segment length and, notably, resisted amyloid beta oligomer (AβO)–induced neuronal activity reduction. Introducing the 1N4R-tau isoform, but not other isoforms, confers AβO vulnerability and increases KxGS phosphorylation of tau, without altering neuronal activity or microtubule modifications.

Mohamed Aghyad Al Kabbani and Michael Bell-Simons contributed equally to this study.

DISCUSSION: While tau KO impacts neuronal development and activity, tau-KO also confers resistance against AβO insult. 1N4R-tau likely mediates AβO-induced and phosphorylated tau toxicity, representing a novel prime therapeutic target for AD.

KEYWORDS
axon initial segment, Alzheimer's disease, amyloid beta, human induced pluripotent stem cells, induced neurons, isoforms, knockout, neuronal activity, tau, tauopathy

Highlights

- Tau knockout alters neurite growth and axon initial segment formation in human neurons.
- Tau isoforms show differential axonal localization in human neurons.
- Tau depletion protects against amyloid beta oligomer (AβO)–mediated neurotoxicity.
- 1N4R tau mediates AβO-induced toxicity in human neurons.

1 | BACKGROUND

The formation of neurofibrillary tangles (NFTs) by hyperphosphorylated tau is the hallmark of Alzheimer's disease (AD) and other neurodegenerative diseases. Under pathological conditions, such as in the presence of toxic amyloid beta (Aβ) oligomers (AβOs), tau becomes hyperphosphorylated, altering axonal microtubule (MT) dynamics, causing axonal transport deficits, synapse loss, and ultimately neuronal death and cognitive decline.[1] In rodents, tau knockout (KO) results only in mild phenotypes and is compensated by the upregulation of other MT-associated proteins (MAPs), such as MAP1A and MAP6.[2,3] Tau KO or suppression in primary neurons causes decreased axonal growth and shorter neurite length, but does not impair axonal transport, MT stability, neuronal activity, or synaptic spines.[4–10] While tau pathology is closely correlated with cognitive decline in AD patients, co-occurring Aβ pathology drives tau accumulation and disease progression.[11–15] Reducing tau levels in animals protects against Aβ-induced neurotoxicity, memory deficits, and premature mortality.[16–20]

Tau regulates axonal MT stability, axonal transport, growth, synapse formation, and other MT-associated processes.[1] In the adult human brain, six tau isoforms originate from alternative splicing of exons 2, 3, and 10 of the *MAPT* gene,[21,22] differing in the number of N-terminal inserts (0N, 1N, or 2N) and C-terminal repeat domains (3R or 4R). During development, human brain tau isoform composition shifts from exclusively 0N3R tau to an equal ratio of 3R to 4R tau.[23–25] Notably, in the adult human brain 1N tau isoforms (1N3R/1N4R) account for 50% of the Tauom, and 2N tau isoforms are the least expressed isoforms (5%–10% of Tauom),[23] while in rodents 2N isoforms account for the majority of expressed tau.[24] In rodents and derived neurons, the isoforms differ in intracellular localization, suggesting isoform-specific tau functions.[26–29] Larger, more mature isoforms, for example, 1N4R and 2N4R, are partially retained in the soma and dendrites.[27,29] The significance of the isoform expression ratio for neuronal health is underscored by mutations in the *MAPT* gene that affect its splicing: Changes leading to an imbalance of 3R to 4R tau expression have been directly associated with frontotemporal dementia (FTD) and tauopathies can be classified by the isoforms present in the pathological NFTs.[30]

Rodents, which express almost exclusively 4R tau isoforms (whereas human neurons express 3R and 4R tau[23,24]), are often used to better understand disease pathology and identify potential therapeutic targets. However, rodents do not naturally develop dementia, and tauopathy models rely on the overexpression of single (mutant/ human) tau isoforms to study disease mechanisms.[31] The establishment of various human neuronal model systems, such as SH-SY5Y-derived neurons, 2D/3D cultures of induced pluripotent stem cell (iPSC)–derived neurons, and human brain organoids already have led to valuable insights into disease pathology and the contribution of tau (reviewed in [1]), but the contribution of the different tau isoforms to tau physiology and toxicity in disease remains unclear. Here, we generated tau KO human iPSCs (hiPSCs) based on the well-characterized WTC11 cell line,[32] modified to be easily differentiated into glutamatergic neurons (iNeurons) using doxycycline-induced expression of the transcription factor neurogenin 2 (Ngn2).[33] Tau KO neurons showed impairments of neurite growth and axon initial segment (AIS) formation, restored by re-expression of individual tau isoforms. Tau KO neurons were protected against AβO-induced neuronal dysfunction and transcriptomic changes, and only the 1N4R tau isoform fully restored the AβO vulnerability of tau KO neurons, based on the higher basal phosphorylation levels of 1N4R tau within the KxGS motif of the MT-binding domain, suggesting that this isoform is less MT bound compared to other isoforms. All in all, we describe a human tau KO neuronal model and identify 1N4R as a critical mediator of tau toxicity in hiPSC-derived neurons, implying 1N4R tau to be a potential therapeutic target for AD.

2 | MATERIAL AND METHODS

2.1 | iPSC maintenance

WTC11 iPSCs with a doxycycline-inducible *Ngn2* transgene[33] were cultured as described previously.[34] In brief, cells were cultured on Geltrex-coated plates (Thermo Fisher Scientific) at 37°C, 5% CO_2 in a humidified incubator and regularly passaged in a 1:10 to 1:20 ratio, using Versene (Thermo Fisher Scientific) and thiazovivin-supplemented StemMACS iPS-Brew X.F. (Axon Medchem and Miltenyi Biotec) for the first 24 hours.

2.2 | Differentiation of hiPSCs into cortical neurons (iNeurons) and co-cultures with primary astrocytes

Differentiation into cortical neurons was performed as described previously with slight modifications.[33–35] At the start of differentiation, cells were harvested using Accutase (Thermo Fisher Scientific) and seeded onto Geltrex-coated plates using a pre-differentiation medium supplemented with thiazovivin (day before differentiation [d] −3). The medium was changed daily for 2 days to a fresh pre-differentiation medium without thiazovivin. On day 0, cells were seeded onto Poly-D-lysine (Sigma-Aldrich)/Laminin (Trevigen)–coated plates using maturation medium supplemented with 1:100 Geltrex. Half of the media was exchanged once per week until analysis.

For the co-cultivation of primary astrocytes with hiPSC-derived neurons, glia cells were harvested using trypsin/ethylenediaminetetraacetic acid (EDTA; PAN-Biotech) and subsequently added to neuronal cultures in a 2:1 ratio of neurons to astrocytes at day 3 to 4 of differentiation. On the next day, cultures were treated with 2 µM cytosine β-D-arabinofuranoside (Ara-C, Sigma-Aldrich), and half of the media was exchanged twice a week afterward. From day 9 onward, 10% fetal bovine serum (FBS, Biochrom AG) was added to the maturation medium to maintain astrocytes.

2.3 | Isolation and cultivation of primary murine astrocytes

Primary murine astrocytes were isolated as described before.[35,36] Brains of FVB/N mouse embryos were dissected at embryonic day 13.5. The whole cortex was digested with trypsin 0.5%/EDTA 0.2% (PAN-Biotech) for 7 minutes at 37°C after removal of the meninges. Then, astrocytes were seeded onto Poly-D-lysine coated T75 flasks and cultivated in a humidified incubator at 37°C, 5% CO_2 in glial plating medium (neurobasal media [Thermo Fisher Scientific], 10% FBS, 1× antibiotic-/antimycotic solution [Thermo Fisher Scientific]). Astrocytes were passaged routinely. The isolation of primary astrocytes was reviewed and approved (according to §4 TschG) by the animal welfare officer of the University of Cologne and the Landesamt für Natur-, Umwelt- und Verbraucherschutz (LANUV), Germany. Co-cultures with primary astrocytes were used exclusively for live-cell calcium imaging experiments.

RESEARCH IN CONTEXT

1. **Systematic review**: We reviewed the literature on tau isoforms, Alzheimer's disease (AD) pathology, and neuronal dysfunction to contextualize our study. Previous research extensively investigated the role of tau in neurodegeneration, particularly in AD. However, human models are scarce and tau toxicity mediation remains enigmatic. Despite the failure of past tau-targeting therapies, human-specific tau isoforms remain understudied, highlighting the necessity of identifying toxic tau subspecies.
2. **Interpretation**: While the tau protein is considered a key driver of AD, the importance of tau isoforms remains understudied. We generated human *MAPT* knockout induced pluripotent stem cell–derived disease-relevant neurons. These neurons are resistant against AD-like insult, but show detectable defects in neuronal physiology. Re-introduction of the 1N4R-tau isoform, but not other tau isoforms, re-established neuronal vulnerability to amyloid beta exposure.
3. **Future directions**: Future tau-based (therapeutic) studies must consider the human-specific tau isoforms and their neuronal functions. Mature tau isoforms are prime targets for AD and related tauopathies.

2.4 | Cultivation of HEK293T cells

HEK293T cells were cultured at 37°C, 5% CO_2 in a humidified incubator and regularly passaged in a 1:10 ratio, using trypsin 0.5%/EDTA 0.2% (PAN-Biotech) and Dulbecco's Modified Eagle Medium, high glucose, GlutaMAX (Thermo Fisher Scientific) supplemented with 10% FBS and 1× antibiotic-/antimycotic solution (Thermo Fisher Scientific).

2.5 | Generation of tau-KO iPSCs

For the generation of *MAPT* (tau) KO iPSCs, two individual guide RNAs (gRNAs) targeting exon 1 of the *MAPT* gene (for gRNA sequences, see Table S1 in supporting information) were cloned into the pX330A-G2P plasmid containing green fluorescent protein (GFP) and puromycin resistance as selection markers.[37] Human iPSCs were seeded using accutase (d0) and transfected with one of the gRNA-containing plasmid 1 day after plating (d1) using Lipofectamine 3000 (Thermo Fisher Scientific) according to the manufacturer's protocol. For the next 3

days, transfected cells were selected using 0.75 µg/mL puromycin (d2–4) until all cells in untransfected (= control) wells were dead. The media was changed to StemMACS iPS-Brew X.F. without puromycin, and cells were recovered for another 3 days. On day 8, single-cell derived colonies were picked and transferred to a GT-coated 96-well plate containing iPS-Brew and 1× RevitaCell (Thermo Fisher Scientific). When cells reached >70% confluence on the 96-well plate, cells were lifted using Versene (Thermo Fisher Scientific) and gentle scraping, and cells were transferred to 24-well plates. When cells again reached >70% confluence on the 24-well plate, cells were transferred to 6-well plates using Versene and gentle scraping. DNA was isolated from all single cell–derived colonies using the InnuPrep DNA mini kit (Analytik Jena); exon 1 of the *MAPT* gene was amplified by polymerase chain reaction (PCR; see Table S1 for sequencing primer) and subsequently sent for sequencing at Microsynth Seqlab (Germany). Three clones harboring homozygous deletions that showed no morphological changes were selected for further KO validation. If not stated otherwise, all subsequent experiments involving tau KO cells were conducted with clone #2.

2.6 | Off-target sequencing

Potential CRISPR/Cas9 gRNA off-target regions (predicted by Benchling's CRISPR Guide RNA Design Tool) were amplified using Phusion polymerase-based PCR (New England Biolabs) according to the manufacturer's protocol (for details on primer sequences, see Tables S2 and S3 in supporting information) and afterward sent for sequencing at Microsynth Seqlab.

2.7 | Karyotyping of *MAPT* KO hiPSC clones

MAPT KO iPSC clones were seeded on Geltrex-coated T25 cell culture flasks (Thermo Fisher Scientific) and cultured in StemMACS iPS-Brew X.F. medium (Miltenyi Biotec) until 70% confluency. The numerical and structural chromosomal constitution of each of the four clones was analyzed by conventional karyotyping using GTG banding (G-bands by trypsin using Giemsa) according to standard protocols. Microscopy was performed with an Axioplan fluorescence microscope (Carl Zeiss) and Neon/Ikaros imaging software (v.6.3.7, MetaSystems). An average of 20 metaphases were analyzed for each clone. Karyotypes were analyzed and reported according to the International System for Human Cytogenetic Nomenclature (ISCN, 2020) with a resolution of 400 to 550 bands per haploid karyotype.

2.8 | Sample preparation for whole proteome analysis by mass spectrometry

WT and tau KO iNeurons were harvested at day 21 of differentiation after treatment with 1 µM AβOs or vehicle control for 3 hours. Cell lysis was performed as described previously[28] and protein amount was determined using the Pierce BCA Protein Assay Kit (Thermo Fisher Scientific). One hundred µg of protein were precipitated using acetone overnight and resuspended in urea buffer (8 M urea in 50 mM triethylammoniumbicarbonate). Afterward, chromatin was degraded using a Bioruptor (Diagenode) and lysates were centrifuged at 20,000 × g for 15 minutes. Proteins were digested following an in-solution digestion protocol. Therefore, dithiothreitol was added to a final concentration of 5 mM and incubated at room temperature (RT) for 1 hour. Chloroacetamine was added to achieve a final concentration of 40 mM followed by incubation at RT for 30 minutes (in the dark). Then, 0.5 µg/µL lysyl endopeptidase was added in an enzyme-to-substrate ratio of 1:75 and incubated for 4 hours at RT. Afterwards, 1 µg/µL trypsin was added in an enzyme-to-substrate ratio of 1:75 and incubated overnight at RT. To stop enzymatic digestion, formic acid was added the next day to a final concentration of 1%. Thirty µg protein of each sample was loaded on a SDB-RP StageTip and handed over to the proteomics core facility Cologne (CECAD, Cologne, Germany) for mass spectrometric analysis and subsequent data analysis.

2.9 | Data acquisition of whole proteome analysis

Samples were analyzed by the CECAD Proteomics Facility on an Orbitrap Exploris 480 (Thermo Fisher Scientific, granted by the German Research Foundation under INST 1856/71-1 FUGG) mass spectrometer equipped with a FAIMS Pro differential ion mobility device that was coupled to an UltiMate 3000 (Thermo Fisher Scientific). Samples were loaded onto a precolumn (Acclaim 5 µm PepMap 300 µ Cartridge) for 2 minutes at 15 µL flow before being reverse-flushed onto an in-house packed analytical column (30 cm length, 75 µm inner diameter, filled with 2.7 µm Poroshell EC120 C18, Agilent). Peptides were chromatographically separated at a constant flow rate of 300 nL/min and the following gradient: initial 6% B (0.1% formic acid in 80% acetonitrile), up to 32% B in 72 minutes, up to 55% B within 7.0 minutes and up to 95% solvent B within 2.0 minutes, followed by column wash with 95% solvent B and re-equilibration to initial condition. The FAIMS Pro was operated at −50 V compensation voltage and electrode temperatures of 99.5°C for the inner and 85°C for the outer electrode.

MS1 scans were acquired from 399 m/z to 1001 m/z at 15k resolution. Maximum injection time was set to 22 ms and the AGC target to 100%. MS2 scans ranged from 400 m/z to 1000 m/z and were acquired at 15 k resolution with a maximum injection time of 22 ms and an AGC target of 100%. DIA scans covering the precursor range from 400 to 1000 m/z and were acquired in 60 × 10 m/z windows with an overlap of 1 m/z. All scans were stored as centroid. In addition to the samples, six gas-phase fractionation (GPF) runs were performed for library building. Here, a sample pool was generated by mixing equal amounts of all samples together. The resulting pool was injected six times using the same liquid chromatography parameters as the samples but each covered only 100 m/z of the total mass range of the samples. In each GPF run, staggered windows of 4 m/z, resulting in nominal 2 m/z windows after demultiplexing, were acquired with a resolution of 30 ke.

2.10 | Sample processing in DIA-NN

Samples were analyzed in DIA-NN 1.8.1.[38] A Swiss-Prot canonical human database (UP5640, downloaded 18/06/21) was used for library building with settings matching acquisition parameters. The library was built using the GPF runs and afterward used to search for the sample runs. For both library building and sample analysis, DIA-NN was run with the additional command line prompt "—report-lib-info." Further output settings were: filtered at 0.01 false discovery rate (FDR), N-terminal methionine excision enabled, maximum number of missed cleavages set to 1, minimum peptide length set to 7, maximum peptide length set to 30, minimum precursor m/z set to 400, maximum precursor m/z set to 1000, cysteine carbamidomethylation enabled as a fixed modification. Afterward, DIA-NN output was further filtered on library *q* value and global *q* value ≤ 0.01 and at least two unique peptides per protein using R (4.1.3). Finally, label-free quantification values were calculated using the DIA-NN R package. Afterward, an analysis of the results was performed in Perseus 1.6.15.[39]

2.11 | RNA isolation and quantitative reverse transcription PCR

Induced wild type (WT) and tau KO neurons were harvested at the indicated time points. RNA was isolated using the PureLink RNA mini kit (Thermo Fisher Scientific) according to the manufacturer's protocol. Afterward, RNA was transcribed into cDNA using the ProtoScript II First Strand cDNA Synthesis Kit according to the manufacturer's guidelines (New England Biolabs). For quantitative reverse transcription PCR (qRT-PCR), 20 ng cDNA was mixed with *MAPT*- or *HPRT*-specific primers (see Table S4 in supporting information for primer sequences) and Power SYBR Green PCR Master Mix (Thermo Fisher Scientific) and subsequently analyzed using a StepOnePlus Real-Time PCR System (Thermo Fisher Scientific) with an annealing temperature of 60°C and 40 cycles. Results were analyzed by the $\Delta\Delta_{CT}$ method and normalized to housekeeper gene *HPRT*. Statistical analysis was performed after testing for normal distribution using a one-way analysis of variance (ANOVA) with correction for multiple comparisons (Tukey test).

2.12 | Immunocytochemistry of iPSCs and iNeurons

To validate that tau KO did not affect the pluripotency of the iPSCs, pluripotency marker expression was monitored using immunocytochemistry. For this, cells were fixed with 3.7% FA/4% sucrose in phosphate-buffered saline (PBS) at RT for 30 minutes. Afterward, cells were permeabilized and blocked for 10 minutes in 5% bovine serum albumin (BSA)/0.2% TX-100 in PBS (both Carl Roth) and stained with a mouse anti-Sox2 or anti-Oct3/4 antibody overnight at 4°C (for antibody details, see Table S5 in supporting information). The next day, coverslips were stained with a secondary antibody coupled to an AlexaFluor dye (Thermo Fisher Scientific) for 1 hour at RT. Coverslips were mounted onto glass slides using Aqua-Poly/Mount (Polysciences) and dried overnight at RT (for further details on the immunofluorescence staining procedure, see Zempel and Mandelkow[40] and Buchholz et al.[41]).

Neuronal cultures were fixed and stained as described above. To validate the absence of tau expression, neurons were stained with two anti-tau antibodies (tau-5 and K9JA), and an anti-MAP2 antibody (see Table S5 for details). All cells were imaged using a wide-field fluorescence microscope (Axioscope 5, Zeiss) and ZenBlue Pro imaging software (V2.5, Zeiss), and images were analyzed using ImageJ software. To analyze levels of Homer1 and F-actin levels, neurites were selected by the NeuroJ plugin[42] and further analyzed using the NeuroCyto toolbox.

2.13 | Live-cell calcium imaging

For live-cell calcium imaging used here as a powerful proxy for neuronal activity, cells were differentiated as described above. On day 2 to 3 of differentiation, mouse primary astrocytes were added to the neurons, and calcium imaging was performed as described previously on day 12 to 14 of differentiation.[35] In brief, iPSC-derived neurons were labeled for 20 minutes with 2 µM Fluo-4 or X-Rhod-1 (both Thermo Fisher Scientific) in maturation medium containing 0.02% Pluronic F127 (Merck Millipore). In addition, neurons were treated with 1 µM AβOs (for preparation, see below) for 1 hour at d20 to 21 before staining with Fluo-4 or X-Rhod-1 (in the case of exogenous tau expression) as indicated and subsequent imaging with an inverted Leica DMi8 microscope. To investigate the effect of tau re-expression in tau KO iNeurons on neuronal activity, cells were transduced with either GFP or an individual isoform together with GFP (see lentiviral transduction protocol below). Time-lapse movies of up to 10 different fields (= acquisition regions of interest [ROIs]) were recorded for 1 minute each (frame rate: 1 Hz) using the Leica LAS X software (v3.7.3). Only neurons were considered for the analysis, and visual discrimination of co-cultured astrocytes for the experiments was based on morphology (astrocytes in culture have different shape, size, and branching patterns), calcium signal intensity (low in astrocytes, high in neurons), calcium signaling pattern (in neurons: whole cell body oscillation, fast oscillations (>5×/minute); in astrocytes: individual processes' calcium waves and slow rate (<1×/minute)). Neurons of all acquisition ROIs were counted and subdivided into active and inactive cells by visual inspection of the presence (= active) or absence (= inactive) of fluorescence intensity (F.I.) changes over time in a blinded manner. The percentage of active cells was calculated as the fraction of active cells from the total cell count in an acquisition ROI. Up to 60 acquisition ROIs (with > 3000 cells) were analyzed for every condition in three to six independent experiments. Statistical analysis was performed after testing for normal distribution using a one-way ANOVA with correction for multiple comparisons (Tukey test). Calcium peak count per minute and height were quantified using an automated R workflow (R

version 4.2.1). Therefore, F.I.s of individual cells of each frame were normalized to the minimum F.I. ($\Delta F_0 / F_0$). Afterward, peaks were automatically detected and counted. A minimum peak height was set to ≥ 0.3 of the normalized F.I. Peak height and peak count were averaged for one independent experiment consisting of up to 10 acquisition ROIs; the experiments were repeated independently three to six times. Statistical analysis was performed after testing for normal distribution using a one-way ANOVA with correction for multiple comparisons (Tukey test).

2.14 | Cell lysis and western blot analysis

For western blot analysis iPSCs and induced neurons were harvested and lysed as described previously.[28] In brief, cells were lysed in RIPA buffer (50 mM HEPES pH 7.6, 150 mM NaCl, 1 mM EDTA, 1% Triton X-100, 0.1% sodium dodecyl sulfate, 0.5% sodium deoxycholate) with freshly added 1× Halt Protease and Phosphatase Inhibitor Cocktail (Thermo Fisher Scientific) for 20 minutes at 4°C. The lysate was centrifuged at 16,000 × g for 20 minutes and subsequently diluted in 3× sodium dodecyl sulfate sample buffer. Proteins were separated using a 10% polyacrylamide gel, transferred to polyvinylidene fluoride membranes, and blocked in 5% BSA in Tris-buffered saline with Tween (TBS-T). Membranes were incubated with the primary antibody overnight at 4°C, washed with TBS-T, and incubated with the corresponding secondary horseradish peroxidase–coupled antibody for 1 hour at RT (antibodies used are listed in Table S5). Enhanced chemiluminescent signals were detected with a ChemiDoc XRS+ system (Bio-Rad) using either the SuperSignal West Pico or Femto ECL solution (Thermo Fisher Scientific).

2.15 | Dephosphorylation of protein lysates

To analyze tau isoform expression via western blot analysis, WT iNeurons were lysed in RIPA buffer (50 mM HEPES pH 7.6, 150 mM NaCl, 1 mM EDTA, 1% Triton X-100, 0.1% sodium dodecyl sulfate, 0.5% sodium deoxycholate) containing cOmplete Protease Inhibitor Cocktail (Sigma-Aldrich). Proteins were dephosphorylated using FastAP Thermosensitive Alkaline Phosphatase (Thermo Fisher Scientific) overnight at RT and subsequently analyzed by western blot analysis.

2.16 | Transfection of iNeurons with tau isoforms

Expression plasmids containing different HA-tagged tau isoforms (0/1/2N and 3/4R) were transfected into tau KO neurons using Lipofectamine2000 (Thermo Fisher Scientific). For this, half of the conditioned medium was removed from the neurons and stored at 37°C. For each well of a 24-well plate, 0.5 µg DNA was diluted in 50 µL OptiMEM (Thermo Fisher Scientific), mixed with 1 µL Lipofectamine2000 (diluted with 50 µL OptiMEM), and incubated at RT for 10 minutes. The transfection mix was added dropwise to the cells. Media was changed to conditioned medium 30 minutes after transfection, and cells were analyzed 3 days after transfection.

2.17 | Lentiviral-based expression of tau isoforms

Human tau isoforms were cloned into the lentiviral expression plasmid pUltra ([43]Addgene #24129). Lentiviral particles were produced in HEK293T cells by co-transfection of pUltra with packaging plasmid psPAX (Addgene #12259) and envelope plasmid pMD2.G (Addgene #12260)[44] using polyethyleneimine (PEI) transfection as described previously.[41] Cell culture supernatant was harvested 3 and 4 days after transfection and stored at −80°C. Differentiated iNeurons were transduced with corresponding lentiviral particles at the indicated time points, and the media was changed 24 hours after lentiviral transduction.

2.18 | Aβ preparation

Aβ40 and Aβ42 powder (21st Century Biochemicals, #AB40-0010 and #AB42-0010 or rPeptide, #A-1153-1 and #A-1163-2) were completely dissolved to 1 mM concentration in Hexafluoro-2-propanol (HFIP, 100%) and aliquoted as described previously.[9] HFIP was evaporated completely using a centrifugational evaporator, and the lyophilized powder was stored at −80°C for later reconstitution.

2.19 | Aβ reconstitution, AβO formation, and treatment of iNeurons

Lyophilized Aβ40 and Aβ42 peptides (for preparation, see above) were reconstituted using 50 mM NaOH and mixed to obtain a molecular ratio of Aβ40/42 of 7:3.[9] Next, PBS and 50 mM HCl was added and immediately mixed, obtaining a final concentration of 100 µM. To induce AβO formation, the Aβ mixture was incubated at 37°C for 1 hour. Finally, induced neurons were treated with 1 µM AβO for indicated time points (1, 3, or 24 hours) for subsequent analysis.

2.20 | Determining AβO toxicity in iNeurons

To assess AβO toxicity, cells were fixed and stained with NucBlue (Thermo Fisher Scientific) after treatment with AβO for 3 and 24 hours. Nuclear shape and density were examined as described before with cells classified as dead if their nuclei appeared condensed and smaller than those of viable cells.[45] Each experiment was repeated 3 to 5 times, analyzing ≈ 100 nuclei per condition. Statistical analysis was performed using two-way ANOVA followed by Tukey multiple comparisons test in GraphPad Prism v10 (GraphPad Software).

2.21 | Effect of AβO on dendritic network

To analyze the effect of AβO exposure to the dendritic network, iNeurons were fixed and stained with NucBlue (Thermo Fisher Scientific) and for the dendritic marker MAP2 (see Table S5) after treatment with AβO for 3 hours. The total MAP2 area was assessed and divided by the number of total nuclei for each ROI. Each experiment was repeated 3 to 5 times, analyzing ≈ 100 cells per condition. Statistical analysis was performed using two-way ANOVA followed by Tukey multiple comparisons test in GraphPad Prism v10 (GraphPad Software).

2.22 | Multielectrode array recordings of neuronal activity and spike analysis

WT and tau-KO iNeurons were differentiated in Poly-D-lysine/laminin-coated 24-Well Plate Epoxy (24W700/100F-288; Microchannel Systems, Reutlingen, Germany) for 21 days as described above. On day 2 to 3 of differentiation, mouse primary astrocytes were added for comparison of different genotypes, but not for assaying AβO-mediated effects due to higher vulnerability in the absence of supporting glia. On day 21, extracellular field potentials were recorded for 2 minutes using the MCS Multiwell-MEA-System (Microchannel Systems) with a sampling rate of 20 kHz. Signals were processed with the Multiwell-Screen software (Microchannel Systems) using high-pass and low-pass Butterworth filters with 0.1 and 3.5 Hz cut-off values, respectively. Signals above or below 5.5× standard deviation were defined as spikes. Spike timestamps were extracted using the for each electrode in each well. Because iNeuron growth in MEA plates was not homogenous, electrodes with a spike rate > 1 Hz were deemed active and considered for subsequent analysis. Wells with < 3 (out of 12) electrodes were excluded from the analyses.

2.23 | Whole transcriptome sequencing (mRNAseq) analysis of AβO-exposed iNeurons

RNA of three independent experiments was isolated from WT and tau KO iNeurons (d21) treated with 1 μM AβOs or vehicle control for 3 and 24 hours as described above (2.11 RNA Isolation and qRT-PCR) and subsequently sent to Novogene Co. (Cambridge, UK) for whole transcriptome paired-end sequencing using the Illumina NovaSeq6000 system.

2.24 | Pseudo-alignment with kallisto

Data was obtained from Novogene Co. (Cambridge, UK) and subdivided into eight groups: KO.AB.24, KO.AB.3, KO.CON.3, WT.AB.24, WT.AB.3, WT.CON.24, and WT.CON.3. Each group has three replicates. All fastq-files were processed with kallisto (version 0.46.0)[46] to make the pseudoalignment using the human GRCh38 cDNA release 109 (https://ftp.ensembl.org/pub/release-109/fasta/homo_sapiens/cdna/) as a reference to build the index.

2.25 | Differential gene expression with DESeq2

To analyze differential gene expression, we used the tximport function[47] to facilitate the output of kallisto in the form of an expression matrix. With DESeDataSetFromTximport, a function from DESeq2 R package,[48] we built a DESeq2 object and filtered rows with a total sum < 10. After that, DESeq function were used with default parameters. With *results* function, we filter genes with a FDR <0.05 and absolute value of fold change |FC| > 1.3.

2.26 | Gene set enrichment analysis with FGSEA

To run the Gene Set Enrichment Analysis, we ranked up all genes from the results function from DESeq2. The metric used to sort all genes was: sign(log2FC)*rank(abs[log2FC]* [−log10(*p*-value)]), where sign is a function to return the signs of numeric elements (−1 to negative numbers and 1 to positive numbers), rank is a function to return the sample ranks of the values, and abs is a function to return the absolute value of a number. With the genes sorted by this metric in decreasing order we use the fgsea function from the fgsea package[49] with stats = 15, maxSize = 400, nPerSimple = 10000 and *P* value < 0.05. The gene set file to run the gsea analysis was the C5 set from Human MsigDB Collections (https://www.gsea-msigdb.org/gsea/msigdb/collections.jsp) which correspond to genes annotated by the same ontology term. This collection is divided into two subcollections, the first derived from the Gene Ontology (GO) resource, which contains BP (Biological Process), CC (Cellular Component), and MF (Molecular Function) components, and the Human Phenotype Ontology (HPO). In this work, we used only the GO sub-collection.

2.27 | Differential transcript usage with IsoformSwitchAnalyzeR

To perform a differential transcript usage (DTU) analysis, we used the R package IsoformSwitchAnalyzeR.[50] In the first part of the pipeline, kallisto abundance matrices were imported with importIsoformExpression and importRdata to create an isoform object. GRCh38 cdna release 109 (same used on kallisto pseudoaligment) were used with the correspondent annotation (https://ftp.ensembl.org/pub/release-109/gtf/homo_sapiens/) release 109. Data was filtered using gene expression cutoff = 10, isoform cutoff = 3, differential isoform fraction (dIF) cutoff = 0.05 and absence of single isoform genes. After that, we used DEXSeq[51] to test differential isoform usage.

In part two of the pipeline, we used fasta files obtained in part one to run external analysis necessary to execute the second part of the algorithm. Outputs of CPC2,[52] Pfam,[53] SignalIP,[54] and Netsurfp2[55] were used as input to isoformSwitchAnalysisPart2. To identify event

consequences, we used the extractConsequenceSummary function to extract gain/loss of predicted functional consequences. Only isoforms with |dIF| < 0.05 and isoform_switch_q_value < 0.01 were considered significant.

2.28 | Tau isoform localization in tau KO iNeurons

To analyze tau axonal enrichment, tau KO iNeurons were transduced with a multi-cistronic lentiviral construct expressing GFP and the corresponding HA-tagged tau isoform as described above. Neurons were fixed after 10 days and stained for the HA-tag and MAP2 as described previously,[40,41] using antibodies listed in Table S5. After imaging on a wide-field fluorescence microscope (Axioscope 5, Zeiss), axonal sorting was analyzed as described previously[28,56] by measuring mean fluorescence intensities (MFI) of GFP and tau in the axon and soma. The experiment was performed in five replicates, and at least 15 cells were analyzed per condition. A Shapiro–Wilk test was performed to test for normal distribution of data; afterward, statistical analysis was performed by one-way ANOVA with correction for multiple comparisons (Tukey test) using GraphPad Prism software (v8.0.1).

2.29 | Analysis of tau isoform stability using cycloheximide

HEK cells were seeded onto 10 cm dishes and transfected with individual HA-tagged tau isoforms[36] using PEI when they reached ≈ 80% confluency. One day after transfection, cells were plated onto 6-well plates, and protein translation was inhibited by treatment with 10 µg/mL cycloheximide (CHX; for 0, 2, 4, and 8 hours) 24 hours after sub-plating. After the indicated time points, cells were harvested and lysed as described above. The obtained proteins were de-phosphorylated using FastAP (Thermo Fisher Scientific) according to the manufacturer's protocol and used for western blot analysis. Exogenous tau isoform expression was monitored using anti-HA antibody and normalized to the loading control β-actin (see Table S5 for details on antibodies used). Band intensity was quantified using Fiji/ImageJ software and plotted depending on the time of CHX treatment. The experiment was repeated independently three times, and a linear regression analysis, followed by a one-way ANOVA with correction for multiple comparisons (Tukey test) after testing for normal distribution, was performed.

2.30 | Neurite outgrowth of iNeurons

To measure neurite outgrowth, iNeurons were transfected with a tdTomato-expressing plasmid at day 1 of the differentiation using Lipofectamine Stem (Thermo Fisher Scientific) or transfected with pUltra plasmids expressing individual tau isoforms together with GFP. Neurons were fixed at days 3, 5, and 7 of neuronal differentiation and imaged using a wide-field fluorescence microscope (Axioscope 5, Zeiss) and the ZenBlue Pro imaging software (V2.5, Zeiss). Neurites were followed by volume marker GFP, and neurite length was measured using Fiji/ImageJ software. The experiment was repeated independently three times; at least 20 cells were analyzed each time. After testing for normal distribution, statistical analysis was performed using an unpaired *t* test (comparing WT and tau KO) or a one-way ANOVA with correction for multiple comparisons (Tukey test; comparing the different tau isoforms) using GraphPad Prism software.

2.31 | AIS length and distance from soma of iNeurons

To measure AIS length and distance from the soma, iNeurons were transduced with lentiviral particles expressing the corresponding tau isoforms at day 7. Neurons were fixed at day 18 of neuronal differentiation, stained with AIS marker TRIM46 as described above, and imaged using a wide-field fluorescence microscope (Axioscope 5, Zeiss) and the ZenBlue Pro imaging software (V2.5, Zeiss). TRIM46 F.I. signal was measured for at least 65 nm of the corresponding axon beginning from the edge of the soma using ImageJ software. Afterward, F.I. was normalized to the maximum F.I. of each axon. A positive TRIM46 signal (= AIS) was determined as an F.I. ≥ 30% of the maximum F.I. The distance between the beginning of the AIS and the edge of the soma was defined as the AIS distance from the soma. Three independent experiments were performed, and ≥ 20 cells were analyzed each time. Statistical analysis was performed after testing for normal distribution either by performing an unpaired *t* test (comparing WT and tau KO) or a one-way ANOVA with correction for multiple comparisons (Tukey test, comparing the different tau isoforms) using Graphpad Prism software.

3 | RESULTS

3.1 | Generation and characterization of tau KO iPSCs

To study the six human brain-specific tau isoforms and their role in tau-associated functions as well as neurodegeneration, we aimed to establish a human-based neuronal model system suitable for the individual characterization of tau isoforms. Therefore, we generated *MAPT* KO human iPSCs (here referred to as tau KO) that can be easily differentiated into highly homogenous cultures of cortical neurons for the functional characterization of the tau isoforms. For this, WTC11 iPSCs with a doxycycline-inducible *Ngn2* transgene[33] were transfected with a Cas9 nuclease and guideRNA (gRNA) co-expressing plasmid (pX330A-G2P, Figure 1A). Two independent gRNAs were designed to target exon 1 of the *MAPT* gene (on chromosome 17), present in all six human brain–specific tau isoforms (Figure 1A, Table S1). After transfection of the iPSCs with one of the two gRNAs, selection with puromycin and single-cell expansion was performed. Exon 1 was amplified from the isolated clones by PCR (Figure S1A in supporting information) and sequenced to confirm the presence of indel mutations that could result

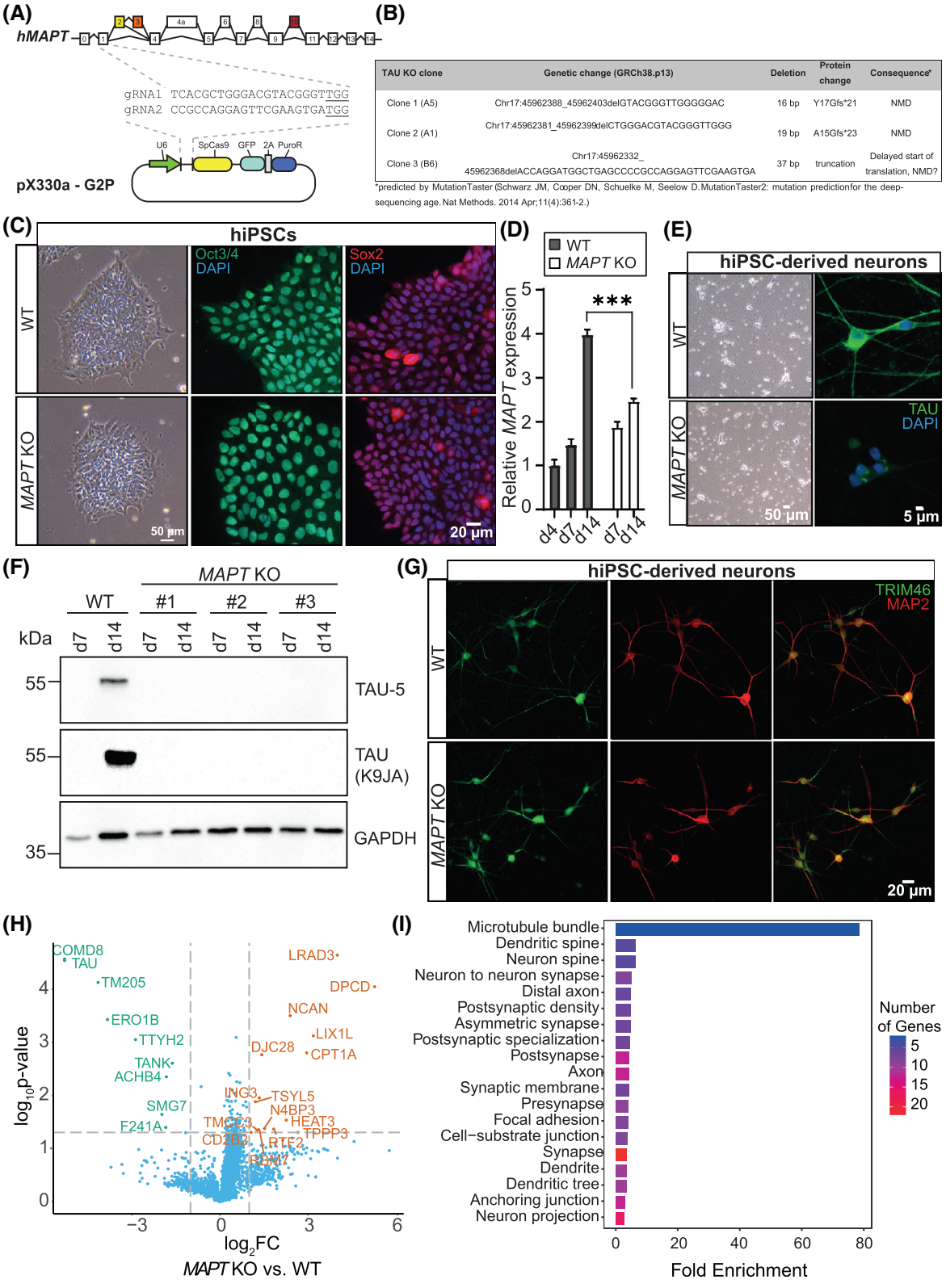

FIGURE 1 Generation of *MAPT* KO hiPSCs using CRISPR/Cas9. A, Schematic representation of CRISPR/Cas9 editing strategy to generate *MAPT* KO (= tau KO) hiPSCs. GuideRNAs (gRNAs) were designed to target exon 1 (which is included in all human tau isoforms; see Table S1 in supporting information for sequences) of the *MAPT* gene and cloned into the Cas9-expressing vector pX330a-G2P, harboring a puromycin resistance (PuroR) as well as a GFP, both serving as selection markers. B, Overview of the generated tau KO clones used in this study. All three clones harbor homozygous deletions in exon 1 of the *MAPT* gene, which likely cause NMD and, subsequently, a PTC. C, Representative brightfield images of WT and tau KO hiPSCs (left panel) and validation of stem cell status by pluripotency markers Oct3/4 (middle panel) and Sox2 (right panel) demonstrate no apparent differences in stem cell properties. D, *MAPT* mRNA expression (measured by qPCR) in hiPSC-derived WT and tau

in frameshift mutations and premature termination codons (PTCs). Seventy-five percent of the total 52 screened clones harbored at least a heterozygous indel mutation. Sequencing revealed three potential KO clones with homozygous deletions in exon 1 (Figure 1B): clone 1 carries a homozygous 16 bp deletion, clone 2 a homozygous 19 bp deletion, and clone 3 a homozygous 37 bp deletion starting already in the 3' intronic region, spanning over the start codon of the *MAPT* gene. Both deletions in clones 1 and 2 in the *MAPT* gene result in frameshifts and subsequent PTC, while a delayed start of translation or nonsense-mediated decay (NMD) could be the consequence of the deletion in clone 3. All transcripts, however, likely undergo NMD, as predicted by the in silico mutation prediction tool MutationTaster.[57]

The three selected iPSC clones were monitored for the absence of phenotypic changes in the undifferentiated state and stained for the pluripotency markers Oct3/4 and Sox2, which ruled out off-target effects of the Cas9 nuclease on stem cell identity (Figure 1C). The top five in silico predicted off-targets of the two gRNAs (see Tables S2 and S3) were amplified and sequenced for all clones and revealed no unwanted edits in these regions in any of the clones (Figure S1B,C). Karyotyping of the original WT iPSC cell line and the tau KO iPSC clones generated in this study revealed that the WT, as well as clones 2 and 3, have a numerically inconspicuous but structurally aberrant karyotype with a derivative chromosome 18 (46, XY, der[18]), while clone 1 has a normal karyotype (Figure S1D).

To monitor *MAPT* mRNA expression, iPSCs were differentiated into glutamatergic neurons (iNeurons) for up to 14 days, using doxycycline-induced *Ngn2* expression as described previously.[34] *MAPT* transcripts were amplified by qRT-PCR (Figure 1D) using an exon 12–specific primer, which is common for all human tau isoforms (see Table S4) and were still detectable after 2 weeks of differentiation but significantly reduced compared to WT levels, suggesting decreased *MAPT* expression or NMD.

Neuronal morphology was assessed by brightfield microscopy (Figure 1E, left panels) and did not reveal apparent differences between WT and tau KO iNeurons (d14). Immunofluorescence staining of iNeurons for dendritic marker MAP2 and AIS marker TRIM46 revealed no apparent differences in neuronal morphology, polarity, or differentiation capacity between the genotypes (Figure 1E,G). Subsequently, the absence of tau expression was confirmed by immunofluorescence staining using a monoclonal antibody against tau (for details, see Table S5), which demonstrated no apparent immunoreactivity in tau KO iNeurons (Figure 1E, right panels).

In addition, the absence of tau protein expression was validated by western blot analysis (Figure 1F) using two tau-specific antibodies (mono- and poly-clonal) recognizing different epitopes. Indeed, none of the three clones expressed tau protein 2 weeks after the start of differentiation. Furthermore, whole proteome analysis revealed a 32-fold reduction of tau protein levels in the tau-KO iNeurons indicative of an efficient depletion of tau protein from iNeurons, but remarkably little change in other proteins, indicating no major physiological changes in tau KO iNeurons (Figure 1H). From the differentially expressed proteins, the majority were associated with MTs, synapses, and dendrites, and involved in 14-3-3 protein binding (Figure 1I).

Compensatory upregulation of other MT-associated proteins, such as MAP1A, has been observed as a direct effect of tau depletion.[1,3] Whole proteome analysis of WT and tau KO iNeurons, however, did not reveal compensatory upregulation of MAP1A or MAP1B protein levels, respectively (Figure 1H), which was further confirmed by immunofluorescence staining (Figure S2A,B in supporting information). Interestingly, while overall *MAP2* gene expression remains unchanged in whole transcriptome analysis (Figure S2C), DTU analysis[50] revealed a significant increase of MAP2c isoform expression but not the other MAP2 isoforms (Figure S2D), which could hint toward more subtle compensatory mechanisms in human neurons compared to rodents. All in all, these results demonstrate the successful generation of tau KO hiPSCs by CRISPR/Cas9 without detectable off-target effects or apparent changes in differentiation capacity, neuronal morphology or polarity, or major protein expression changes compared to WT iNeurons.

3.2 | Tau KO neurons have mild deficits in neurite outgrowth and AIS formation but show robust spontaneous calcium oscillations

To further characterize tau KO iNeurons, tau KO iPSCs were differentiated using doxycycline-inducible *Ngn2* expression as described previously (Figure 2A).[34] Neurite length was assessed at different time points of the differentiation (days 3, 5, and 7) and revealed a significantly reduced neurite length for tau KO iNeurons 1 week after the

KO neurons (iNeurons) shows a clear reduction after neuronal differentiation for 14 days. Error bars represent SEM. Shapiro–Wilk test was performed to test for normal distribution; afterward, statistical analysis was performed by one-way ANOVA with correction for multiple comparisons (Tukey test). Statistical significance: $^{***}P \leq 0.001$. E, Tau KO iNeurons show normal neuronal morphology in brightfield images (left panel) but lack detectable tau expression in immunofluorescence staining using a monoclonal anti-tau antibody (right panel, Table S5 in supporting information). F, Absence of tau protein expression was validated in iNeurons of all three tau-KO clones by western blot analysis. G, Overview immunofluorescence stainings of WT (upper panels) and tau KO iNeurons (lower panels) for the neuronal dendrite marker MAP2 (red), and AIS marker TRIM46 (green) show no apparent differences in neuronal morphology, polarity, or differentiation capacity between the genotypes. H, Volcano plot of differentially regulated proteins identified in tau KO iNeurons compared to WT iNeurons using whole proteome analysis. I, Analysis of GO cellular component of differentially expressed proteins in tau KO iNeurons indicating that most changed proteins are associated with MTs, synapses, and dendritic spines. AIS, axon initial segment; ANOVA, analysis of variance; GFP, green fluorescent protein; GO, Gene Ontology; hiPSCs, human induced pluripotent stem cells; KO, knockout; NMD, nonsense-medicated decay; PTC, premature termination codon; qPCR, quantitative polymerase chain reaction; SEM, standard error of the mean; WT, wild type

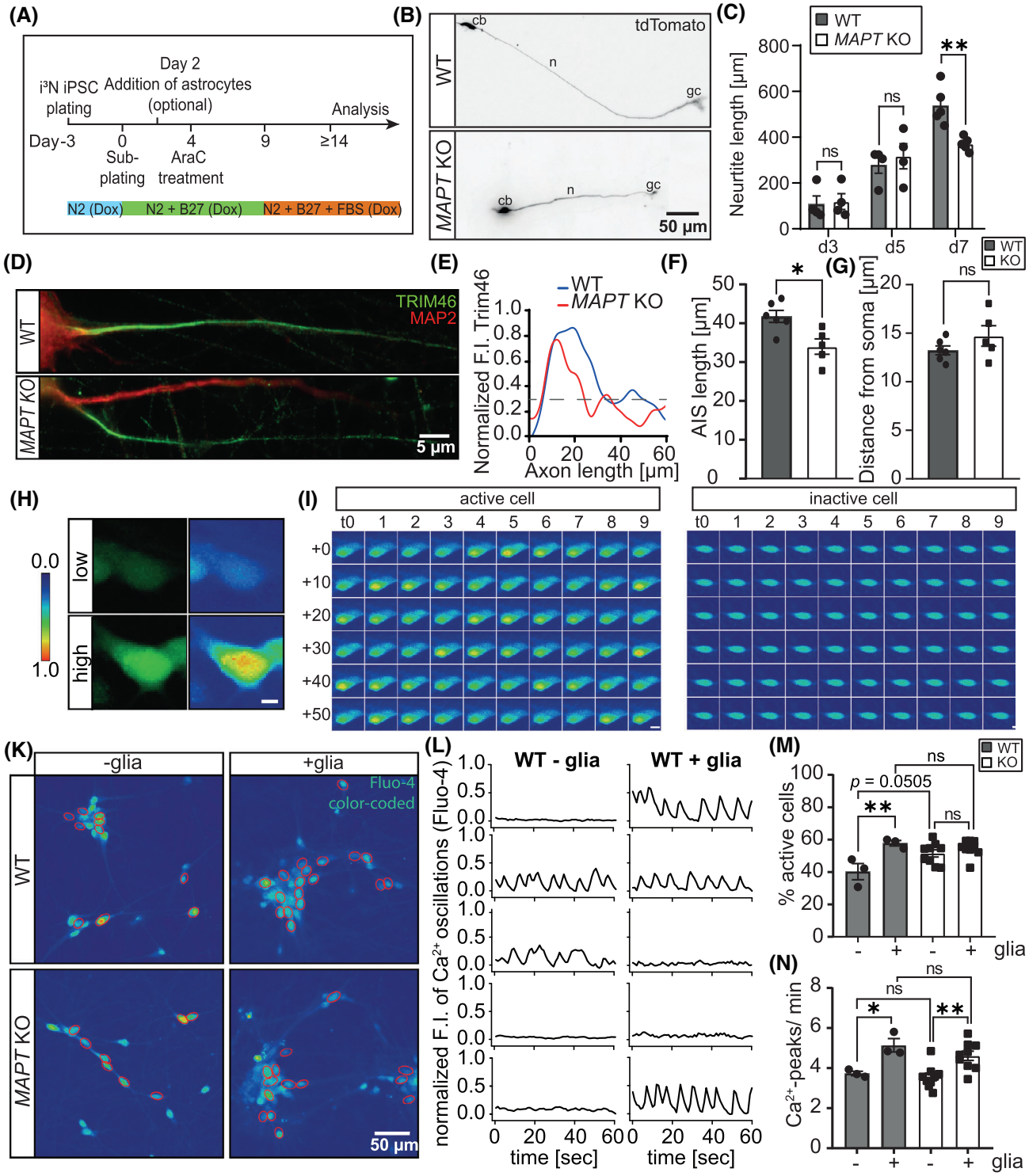

FIGURE 2 Knockout of tau causes mild deficits in neurite growth and AIS formation but does not alter neuronal activity. A, Schematic overview of the differentiation protocol for hiPSCs into glutamatergic neurons based on the doxycycline-induced expression of transcription factor *Ngn2*.[35,36] B, Representative fluorescence images of WT (stitched) and tau KO iNeurons (d7) transfected with tdTomato, indicating reduced neurite length of tau KO iNeurons. C, Quantification of neurite length of WT and tau KO iNeurons 3, 5, and 7 days after the start of differentiation demonstrate reduced neurite extensions only after d7. Error bars represent SEM; Shapiro–Wilk test was performed to test for normal distribution; afterward, statistical analysis was performed by one-way ANOVA with correction for multiple comparisons (Tukey test). $N = 4$, $n = 20$. Statistical significance: $^{**}P \leq 0.01$. D, Representative immunofluorescence images of WT and tau KO iNeurons stained for the axon initial segment marker TRIM46 (green) at d18 of differentiation. Axons were defined by the absence of MAP2 (dendritic marker, red) signal and the presence of TRIM46 staining. E, Representative profile of normalized Trim46 signal from the AIS depicted in (D). The AIS was defined as a TRIM46 signal > 0.3 of the maximum F.I. Quantification of the AIS length (F) and distance from soma (G) in d18 WT and tau KO iNeurons: tau KO leads to reduced AIS

beginning of the differentiation; however, there were no differences at earlier time points (Figure 2B,C).

Impairments in AIS formation have been described in tau knockdown human neurons.[10] To evaluate AIS length and distance from soma, iNeurons were stained for the AIS marker TRIM46 at d18 (Figure 2D–G). Compared to WT iNeurons, tau deficiency resulted in a significant reduction of the AIS length from 41.76 ± 3.78 µm to 34.00 ± 4.38 µm, respectively (Figure 2F). The distance from the soma remained unchanged in tau KO iNeurons (Figure 2G).

After observing deficits in neurite outgrowth and AIS formation, we next analyzed spontaneous calcium oscillations as a proxy for neuronal activity as a functional readout using live-cell calcium imaging as described previously (Figure 2H–K).[35] For this, WT and tau KO iNeurons were loaded with the fluorescent cell–permeable calcium-sensitive dye Fluo-4 on day 12 to 14 of differentiation (Figure 2H–K). Neuronal activity was determined as the percentage of active cells from all recorded cells in an acquisition ROI. Active cells were categorized by visual changes in F.I. of the Fluo-4 signal over time, which represents calcium oscillations (Figure 2I), while inactive cells were determined by a constant low F.I. and the absence of calcium oscillations (Figure 2J). In addition, the F.I. was plotted over the recorded time to confirm the visual categorization of active and inactive cells (Figure 2L). A slight increase (≈ 10%) in overall network activity was observed for tau KO neuronal cultures compared to WT iNeurons (Figure 2M). Of note, WT neurons showed a significantly increased activity (up to ≈ 30%) when co-cultured with primary astrocytes (Figure 2H), which is in line with previous reports.[58]

Interestingly, no significant difference in the overall activity was observed between WT and tau KO lines when co-cultured with primary astrocytes (Figure 2M). Notably, comparable spontaneous calcium oscillations were observed for all three tau KO lines (Figure S3A,B in supporting information), and was consistent and independent of cellular density (Figure S3C,D). To further characterize the active cells, calcium peak frequency and height were analyzed using an automated workflow (Figure 2I,K, Figure S3E). In line with the overall neuronal network activity, peak frequency increased significantly for both WT and tau KO iNeurons, when co-cultured with primary astrocytes (Figure 2K,M, Figure S3E). Peak frequency and height were compared between WT and tau KO neurons using isolated cultures and co-cultures with glia cells but did not reveal any differences between both genotypes (Figure 2N, Figure S3E). While calcium oscillations for iNeurons are a robust proxy and a powerful method for measuring neuronal activity, we also tested whether we could detect differences using a more direct electrophysiological approach using multielectrode array (MEA) analysis. WT and tau KO neurons with glial support showed a trend toward an increased spike rate in tau KO iNeurons (Figure S3F). This may hint toward possibly higher excitability in some circumstances in tau KO iNeurons comparable to the spontaneous calcium oscillations, but in both cases analysis did not meet statistical significance. In sum, while tau depletion leads to mild deficits in neurite growth and a change in AIS length, it did not cause significant alterations in overall neuronal activity or individual neuronal firing rates in human cortical neurons.

3.3 | Tau isoforms are differentially localized in tau KO iNeurons

Recent results from murine primary neurons exhibited a difference in the subcellular localization of tau isoforms.[27,28] To investigate the localization in human neurons, tau KO iNeurons were transduced with HA-tagged tau isoforms at day 7 (Figure 3A,B). Co-expressed GFP was used as a volume marker. After fixation at d21, neurons were stained using an anti-HA antibody, and MAP2 was used as a dendritic marker. Tau axonal enrichment was calculated by normalizing the axonal and somatic fluorescence signals of tau^{HA} to the unbiased levels of GFP as a reliable measure of axonal enrichment, as described in detail previously.[28] In line with previous studies,[28,56] all reintroduced tau isoforms were efficiently sorted into the axon, but none of the re-expressed isoforms reached the axonal sorting efficiency of endoge-

length but may not change the distance from soma. Error bars represent SEM; Shapiro–Wilk test was performed to test for normal distribution; afterward, statistical analysis was performed by a two-tailed unpaired *t* test. $N = 4$, $n = 20$. Statistical significance: $^{*}P \leq 0.05$, ns, not significant. H, Example images of an inactive cell (characterized by low levels of Fluo-4, upper panels) and an active cell (characterized by elevated levels of Fluo-4, lower panels); scale bar = 5 µm. Serial images of an active (I) and an inactive cell (J) over the whole recording period, from $t = 0$ seconds to $t = 60$ seconds as indicated; scale bar = 10 µm. K, Representative images of WT and tau KO iNeurons stained with calcium sensor Fluo-4 (pseudo-colored). Red circles mark active cells, characterized by spontaneous calcium oscillations. L, Exemplary traces of Fluo-4 signal intensity over 1 minute of WT and tau KO iNeurons, indicating spontaneous calcium oscillations and no differences in peak frequency or height between genotypes. M, Quantification of the percentage of active cells within neuronal cultures as assessed by live-cell calcium imaging of WT and tau KO iNeurons (d14) in dependence of co-cultures with primary astrocytes (= glia) showing increased neuronal activity of WT iNeurons, when cells are co-cultured with astrocytes. Tau KO iNeurons show higher neuronal activity when cultured alone but not when co-cultured with astrocytes. Error bars represent SEM; Shapiro–Wilk test was performed to test for normal distribution; afterward, statistical analysis was performed by two-way ANOVA with correction for multiple comparisons (Tukey test). $N = 3–9$, $n > 3000$. Statistical significance: $^{*}P \leq 0.05$, $^{**}P \leq 0.01$, $^{***}P \leq 0.001$, ns, not significant. N, Calcium peak count per minute compared between both genotypes in dependence of co-cultures with primary astrocytes shows that co-cultures with glia cells increase calcium peak frequency of WT and tau KO iNeurons. Error bars represent SEM; Shapiro–Wilk test was performed to test for normal distribution; afterward, statistical analysis was performed by two-way ANOVA with correction for multiple comparisons (Tukey test). $N = 3–9$, $n > 3000$. Statistical significance: $^{*}P \leq 0.05$, $^{**}P \leq 0.01$, $^{***}P \leq 0.001$. AIS, axon initial segment; ANOVA, analysis of variance; cb, cell body; F.I., fluorescence intensity; gc, growth cone; hiPSCs, human induced pluripotent stem cells; KO, knockout; n, neurite; SEM, standard error of the mean; WT, wild type

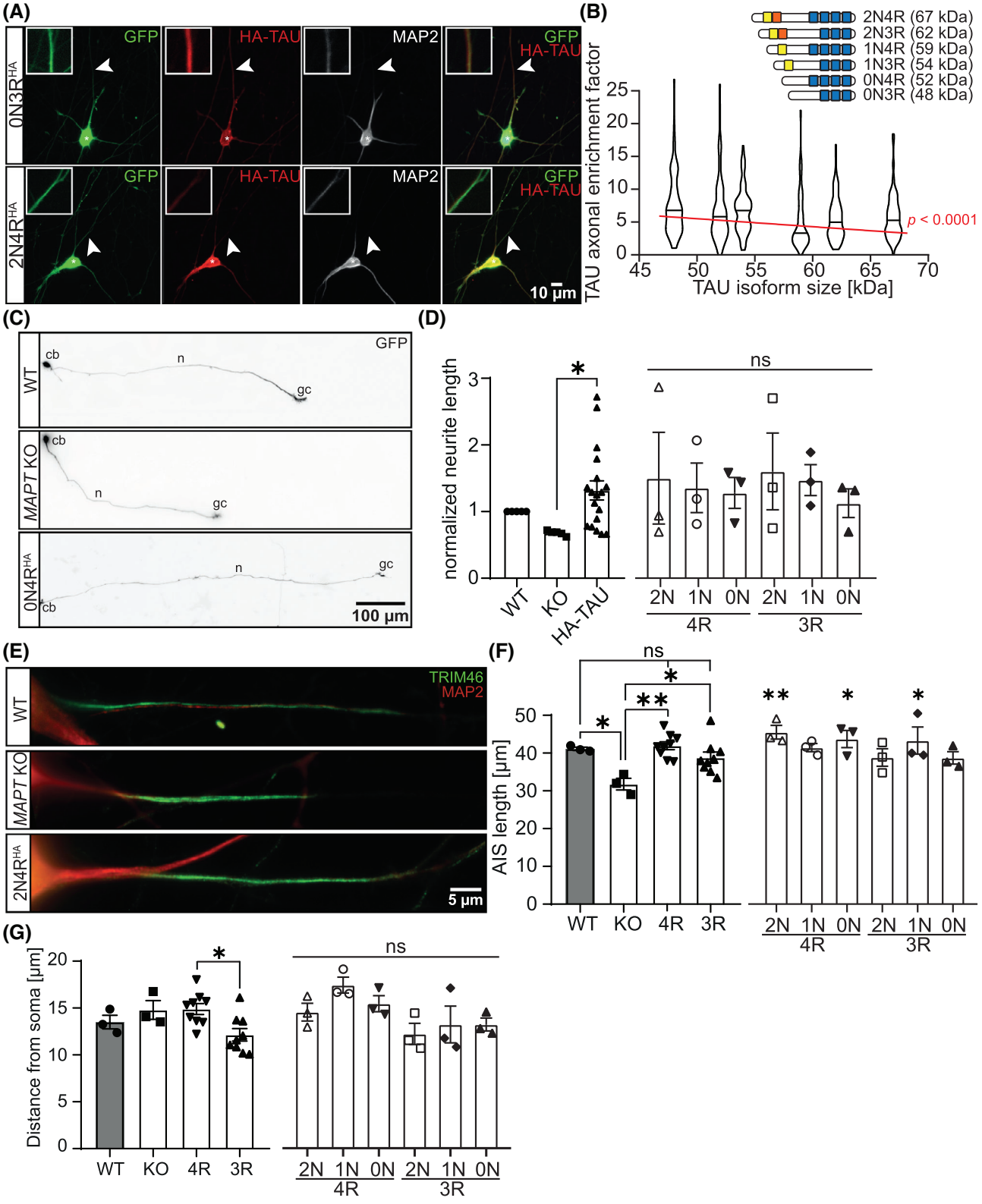

FIGURE 3 Re-expression of tau isoforms in tau KO iNeurons rescues deficits in neurite outgrowth and AIS formation. A, Representative IF images of tau KO iNeurons transduced with either 0N3R^{HA} (middle panels) or 2N4R^{HA} tau (lower panels) together with GFP as a volume marker. Boxes show 9-fold magnified and 5-fold enhanced contrast of (dashed) regions indicated by arrowhead. Larger tau isoform show less axonal targeting than smaller tau isoforms. B, Correlation of tau isoform size (in kDa) with the efficiency of axonal sorting indicates that axonal enrichment depends on tau isoform size. The red line represents the linear regression, which shows a significant incline. The bars on the top right represent the individual isoforms, which differ in the number of N-terminal inserts (yellow and red boxes) and the number of C-terminal repeats (represented by blue boxes) and harbor different protein masses. C, Representative images of WT and tau KO iNeurons transduced with GFP (as a

nous tau (as measured in d21 WT iNeurons; Figure S3G–I). Endogenous tau, which is composed mainly of the shortest isoforms of tau, 0N3R and 0N4R, in WT iNeurons (Figure S3J), is strongly sorted into the axons, as measured by the ratio between axonal and somatic tau levels and normalized to the unbiased distribution of GFP, which is used as a volume marker (Figure S3J). In line with endogenous tau, the shortest isoforms, 0N3R and 0N4R tau, are sorted most efficiently into the axon when re-expressed in tau KO iNeurons. In particular, the bigger isoforms, such as 2N4R, 1N4R, and 2N3R, were partially retained in the soma (Figure 3A,B). Even if the overall sorting of the isoforms does not differ significantly, there is an inverse correlation between the size (also corresponding to the maturity) of the tau isoforms and their axonal enrichment (Figure 3B). The differential sorting efficiency does, however, not perfectly align with the size differences, indicating that size alone cannot account for the differences in sorting.

Turnover rates of proteins in general and of tau, in particular, depend on the subcompartmental localization, but sorting also depends on protein turnover.[59] To test whether differences in the half-life of the tau isoforms may influence the intracellular distribution, CHX treatments were performed in HEK293 cells transfected with individual tau isoforms to assess their turnover rates/half-life independent of neuronal subcompartment localization. The expression levels of tau isoforms were analyzed by using a western blot and revealed no statistically significant differences between the individual tau isoforms (Figure S4A in supporting information). Thus, while all isoforms localize to the axon, axonal sorting efficiency significantly correlates inversely with the tau isoform size.

3.4 | Expression of all individual tau isoforms rescues deficits in neurite growth and AIS formation

To validate that the alterations observed in tau KO iNeurons are directly linked to the depletion of tau, individual tau isoforms were re-expressed in tau KO iNeurons using either liposome-based transfection or lentiviral transduction (Figure S4B). First, we tested which isoform could re-establish proper neurite development in tau KO iNeurons. Therefore, tau isoforms were re-expressed in tau KO iNeurons using liposome-based transfection at d1, and neurite outgrowth was analyzed as described previously. Tau re-expression restored the neurite length to WT levels for all six isoforms (Figure 3C,D). However, no statistically significant changes could be observed between the individual isoforms, indicating that all tau isoforms mediate neurite elongation in our model system. In addition, AIS length was analyzed after the re-expression of tau isoforms for 10 days. All 3R and 4R isoforms restored AIS length of tau KO iNeurons (Figure 3E,F). On the individual isoform level, a statistically significant increase in neurite length was observed for iNeurons expressing 2N4R, 0N4R, and 1N3R compared to tau KO iNeurons (Figure 3F).

No significant influence of the tau isoforms on the AIS distance from the soma was observed (Figure 3G). However, a small but statistically significant difference can be noticed between iNeurons expressing 3R and 4R tau isoforms. 3R isoforms cause a reduction of the distance to the soma compared to iNeurons re-expressing 4R tau isoforms (Figure 3G). In sum, the re-expression of individual isoforms was sufficient to rescue the reductions of AIS and neurite length in tau KO human neurons, indicating that the phenotypes are directly linked to tau loss. Depending on the isoform expressed, minor differences in the rescue efficiency were noticed, which could hint toward isoform-specific functions of tau in human neurons but could also mean that the tau isoforms, to a certain extent, compensate for each other for key aspects of tau function.

3.5 | Tau KO iNeurons are protected against AβO-induced reduction of spontaneous calcium oscillations

Depletion of tau is known to protect AD mouse models and primary neurons derived from these animals against Aβ-induced toxicity.[1,9,16,60] To model AD-like stress in our neuronal cultures, WT iNeurons were treated with an oligomeric preparation of a 7:3 ratio of Aβ40/Aβ42 (Figure 4A,B). Previous reports showed that a ratio of 7:3 of Aβ40 to Aβ42 peptides generates toxic oligomers that potently induce hallmarks of AD, such as tau mis-sorting and hyperphosphorylation in rodent primary neurons.[9,61] Three hours of treatment were sufficient to induce pathological mis-sorting of tau in human WT iNeurons, indicating that AβOs can be used in these cells to study the pathomechanism of AD (Figure 4A,B). Furthermore, whole transcriptome analysis of WT iNeurons after 3 and 24 hours of AβO exposure reveals that exposure to AβOs for 3 hours leads to a significant change in genes involved in stress response, synapse maintenance, and cell adhesion

volume marker), as well as tau KO iNeurons, transduced with 0N4R^{HA} tau and GFP (images were stitched using ImageJ), indicating restored neurite length for tau KO iNeurons expressing 0N4R^{HA} tau. D, Neurite length was quantified after re-expression of individual tau isoforms in tau-KO iNeurons and shows that all isoforms can restore the deficits in neurite outgrowth (significant when all isoforms are pooled). Error bars represent SEM. Shapiro–Wilk test was performed to test for normal distribution; afterward, statistical analysis was performed by one-way ANOVA with correction for multiple comparisons (Tukey test). $N = 3–5$, $n = 15–20$. Statistical significance: $^{*}P \leq 0.05$, ns, not significant. E, Representative IF images of AIS marker Trim46 and dendrite marker MAP2 in WT, tau KO iNeurons, and tau KO iNeurons expressing 2N4R^{HA} tau. AIS length (F) and distance from soma (G) were quantified for WT, tau KO, and re-expressed tau isoforms in d18 iNeurons. Tau expression tends to increase AIS length and may alter the AIS distance from the soma. Error bars represent SEM. Shapiro–Wilk test was performed to test for normal distribution; afterward, statistical analysis was performed by one-way ANOVA with correction for multiple comparisons (Tukey test). $N = 3$, $n = 20$. Statistical significance: $^{*}P \leq 0.05$, $^{**}P \leq 0.01$, $^{***}P \leq 0.001$, ns, not significant. AIS, axon initial segment; cb, cell body; gc, growth cone; GFP, green fluorescent protein; IF, immunofluorescence; KO, knockout; n, neurite; SEM, standard error of the mean; WT, wild type

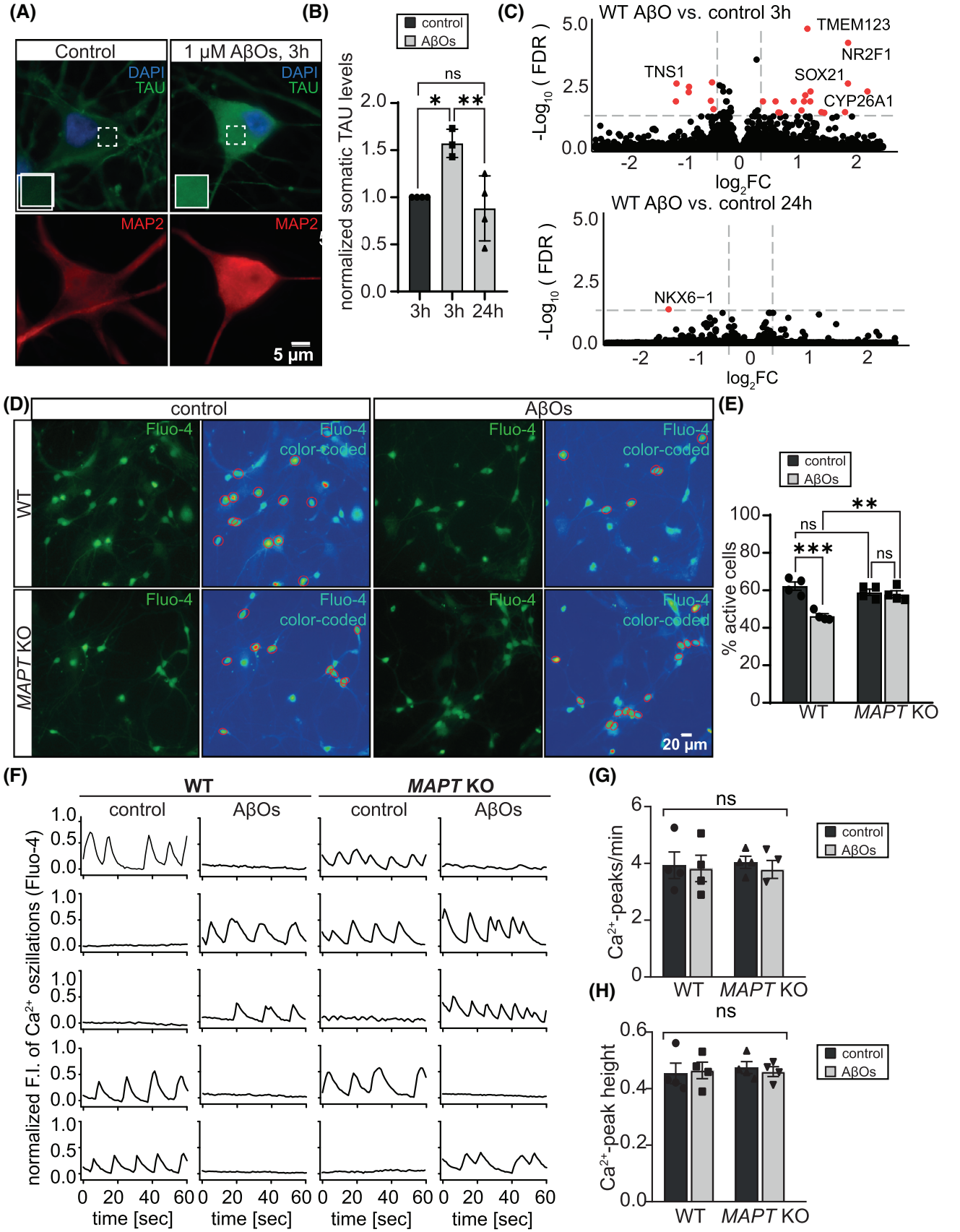

FIGURE 4 Tau KO iNeurons are protected against AβO-induced reduction of neuronal activity. A, Representative IF images of WT iNeurons (d21) treated either with a vehicle control or 1 μM AβOs for 3 hours. Compared to control cells, neurons treated with AβOs showed increased somatic levels of tau. Inlets show magnification of the neurons' somata (boxed area). B, Quantification of the somatic levels of tau in WT iNeurons after treatment with a vehicle control or 1 μM AβOs for 3 and 24 hours. Treatment with AβOs for 3 hours is sufficient to induce pathological

(Figure 4C, Figure S5 in supporting information). Of note, these effects were almost completely reversed after 24 h of exposure. In addition, tau mis-sorting was initially observed after 3 h of AβO exposure, but was not apparent after 24 h (Figure 4B), in line with the absence of direct cytotoxicity caused by AβO exposure (Figure S6A in supporting information). These results confirm previous observations, suggesting that AβOs lose their toxicity over time due to the formation of non-toxic aggregates that are not able to bind to neurons anymore.[9] To investigate the effect of tau loss on neuronal activity, live-cell calcium imaging, and MEA analysis after acute treatment with 1 µM AβOs was performed as outlined above (Figure 4D–H, Figure S6B). While we did not find statistically significant alterations of the electrophysiological activity of the iNeurons after AβO exposure using the MEA analysis (Figure S6B), a significant reduction of neuronal network activity from 62% to 46% of active neurons was observed in the live-cell calcium imaging for WT iNeurons upon AβO exposure (Figure 4D–H). Remarkably, AβO treatment did not affect spontaneous calcium oscillations of tau KO neurons (59% and 58% active cells, respectively), which highlights the protective function of tau KO as well as its key role in driving disease pathogenesis as described for tau KO mice and derived primary neurons.[16,60] However, there was no effect of AβO treatment and tau loss on the individual neuronal activity parameters calcium peak frequency and height (Figure 4D–H).

3.6 | 1N4R tau confers vulnerability of tau KO iNeurons to Aβ-mediated neuronal dysfunction

To understand which isoforms mediate the impairing effects of AβOs on neuronal activity as assayed via calcium imaging, individual tau isoforms were expressed in tau KO iNeurons (using lentiviral transduction at d7) for 14 days, and live-cell calcium imaging was performed, due to the expression of the GFP as a transduction marker, here, using the red fluorescent cell-permeable calcium sensor X-Rhod-1 (Figure 5A). Under basal conditions, a slight but significant reduction of spontaneous calcium oscillations was observed for tau KO iNeurons expressing 1N3R and 0N3R, while the other isoforms did not cause any changes in neuronal activity (Figure 5B,D). Next, neurons expressing the individual tau isoforms were treated with AβOs for 1 hour before live-cell calcium imaging was performed (Figure 5A,C,D). After treatment with AβOs, iNeurons expressing 0N4R, 2N4R, or one of the 3R tau isoforms showed only a mild and not statistically significant reduction of spontaneous calcium oscillations, indicating that the neurons remained partially protected from the AβO-induced decrease in neuronal activity that was observed for WT iNeurons (Figure 5C). Only 1N4R tau was able to fully and significantly confer vulnerability of tau KO iNeurons to AβOs (Figure 5A,C,D). Interestingly, no effect of 1N4R expression was observed on individual neuron activity, as assessed by calcium peak count per minute and calcium peak height of active cells (Figure 5D–F). In agreement with previous results from us and others, we also did not find overt effects on general neuronal viability, or effects on neuronal morphology by AβOs (Figure S6A,C). Also, in line with previous results, the expression of the different isoforms did affect dendrite volume depending on the isoforms, but this was not impacted by AβOs, again showing that AβOs do not cause overt neuronal death, obvious dedifferentiation, or dendrite loss/retraction (Figure S6C). To further investigate how 1N4R could mediate AβO-induced tau-mediated neuronal impairment, we assessed several pathways that have been shown to significantly contribute to neurodegeneration in a tau-dependent manner. Again, tau isoforms were investigated in an isolated context in tau KO iNeurons and compared to each other. No detectable differences in the levels of extracellular glutamate receptor 2 (GluR2), and intracellular postsynaptic density scaffolding protein Homer-1 could be observed between WT, tau-depleted and neurons re-expressing 0N3R or 1N4R tau isoforms (Figure S6D–E). Furthermore, tau isoforms do not affect the levels and distribution of filamentous actin (F-actin) as assessed by a fluorescently labeled F-actin marker (Phalloidin) in tau KO iNeurons compared to tau KO and WT iNeurons (Figure S6F). Tau hyperphosphorylation is a key hallmark observed in tauopathies, causing the dissociation of tau from neuronal MTs, directly affecting axonal transport and synapse function and contributing to the accumulation of

mis-sorting of tau. Error bars represent SEM. Shapiro–Wilk test was performed to test for normal distribution; afterward, statistical analysis was performed by one-way ANOVA with correction for multiple comparisons (Tukey test). $N = 3–4$, $n = –30$. Statistical significance: $^{*}P \leq 0.05$, $^{**}P \leq 0.01$, $^{***}P \leq 0.001$, ns, not significant. C, Volcano plot of DEGs of WT iNeurons treated with vehicle control or AβOs for 3 and 24 hours, respectively, assessed by bulk RNAseq. D, Representative images of WT and tau KO iNeurons (d21) stained with calcium sensor Fluo-4 after treatment with AβOs for 1 hour. Red circles mark active cells, characterized by spontaneous calcium oscillations. E, Quantification of the percentage of active cells in cultures of WT and tau KO iNeurons (d21) after acute treatment with AβOs for 1 hours. WT neurons show reduced neuronal activity after treatment with AβOs, while there is no effect on tau KO neuronal activity. Error bars represent SEM. Shapiro–Wilk test was performed to test for normal distribution; afterward, statistical analysis was performed by two-way ANOVA with correction for multiple comparisons (Tukey test). $N = 3–4$, $n > 1500$. Statistical significance: $^{*}P \leq 0.05$, $^{**}P \leq 0.01$, $^{***}P \leq 0.001$, ns, not significant. F, Exemplary traces of Fluo-4 signal intensity over 1 minute of WT and tau KO iNeurons treated with a vehicle control or AβOs for 1 hour, indicating spontaneous calcium oscillations and no differences in peak frequency or height between genotypes and treatments. G, Calcium peak count per minute quantified for WT and tau KO iNeurons after treatment with AβOs for 1 hour. Error bars represent SEM.; Shapiro–Wilk test was performed to test for normal distribution; afterward, statistical analysis was performed by two-way ANOVA with correction for multiple comparisons (Tukey test). $N = 3–4$, $n > 1500$. Ns, not significant. H, Calcium peak height after 1 hour treatment of WT and tau KO iNeurons with AβOs. Error bars represent SEM. Shapiro–Wilk test was performed to test for normal distribution; afterward, statistical analysis was performed by two-way ANOVA with correction for multiple comparisons (Tukey test). $N = 3–4$, $n > 1500$. Ns, not significant. AβO, amyloid beta oligomer; ANOVA, analysis of variance; DEGs, differentially expressed genes; IF, immunofluorescence; KO, knockout; SEM, standard error of the mean; WT, wild type

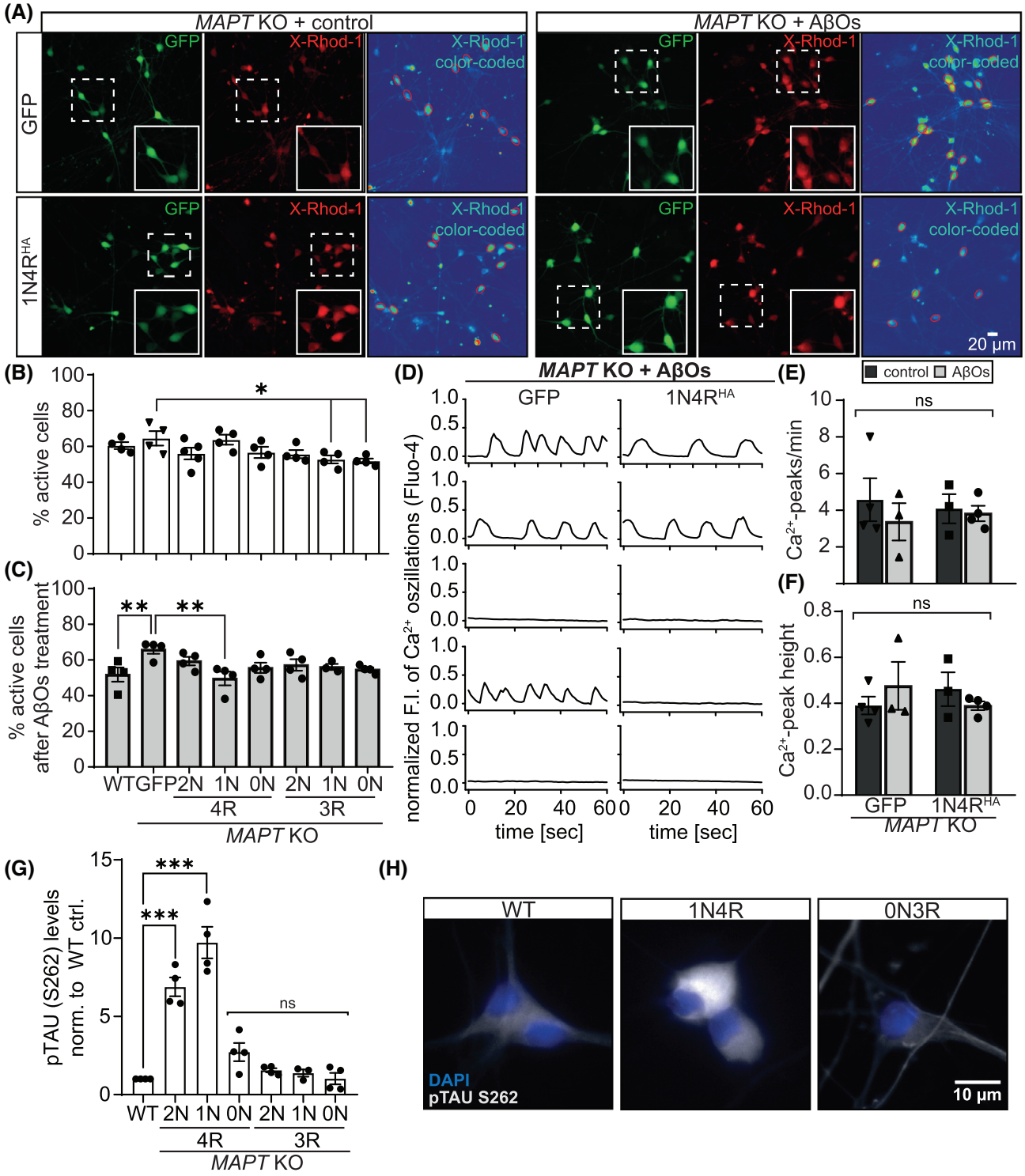

FIGURE 5 1N4R tau restores vulnerability of tau KO iNeurons to AβO-induced neuronal activity reduction. A, Representative images of tau KO iNeurons (d21) expressing either GFP (upper panels) or GFP together with 1N4R tau (lower panels). Neurons were stained with calcium sensor X-Rhod-1 after treatment with a vehicle control or AβOs for 1 hour. Red circles mark active cells, characterized by spontaneous calcium oscillations, inlets (boxed areas) show a 4-fold magnification of cells. B, Quantification of the percentage of active cells in cultures of WT and tau KO iNeurons (d21) re-expressing either GFP or individual tau isoforms. Tau KO iNeurons expressing either 1N3R or 0N3R show reduced neuronal activity compared to tau KO iNeurons expressing GFP. Error bars represent SEM. Shapiro–Wilk test was performed to test for normal distribution; afterward, statistical analysis was performed by two-way ANOVA with correction for multiple comparisons (Tukey test). $N = 4$, $n > 1500$. Statistical significance: $^{*}P \leq 0.05$, $^{**}P \leq 0.01$, $^{***}P \leq 0.001$, ns, not significant. C, Quantification of the percentage of active cells in cultures of WT and tau KO iNeurons (d21) re-expressing either GFP or individual tau isoforms after acute treatment with AβOs for 1 hour. Re-expression of 1N4R-tau re-sensitized tau-KO iNeurons to AβO-induced reduction of neuronal activity. Error bars represent SEM. Shapiro–Wilk test was performed to test for normal distribution; afterward, statistical analysis was performed by two-way ANOVA with correction for multiple comparisons (Tukey test).

tau in the somatodendritic compartment.[62] In particular, phosphorylation at the KxGS motifs (located within the MT-binding domain), has been implicated in the local disruption of MT stability and subsequent synapse loss observed in AD.[9] Therefore, phosphorylated tau levels at serine 262 were assessed for the individual tau isoforms (Figure 5G,H). While the levels of pS262 of 3R tau isoforms and 0N4R tau remained comparable to the levels in WT iNeurons that mainly express 0N4R, 1N4R and 2N4R isoforms were highly phosphorylated in tau KO iNeurons already under basal conditions (Figure 5G,H). We next analyzed tubulin posttranslational modifications (PTMs) as a readout for MT stability and dynamics (Figure S6G,H). We assessed tubulin acetylation (Ac) as a marker for stable but flexible MT[63] and tubulin polyglutamylation (polyE), which leads to the recruitment of MT-severing enzymes, such as SPASTIN, as a marker for less stable and more dynamic MTs.[64] On basal levels, MT PTMs were not significantly changed upon tau depletion in iNeurons, further underlining the likely compensation of other MT-associated proteins. Upon AβO exposure for 3 hours, a trend toward less Ac-tubulin and more polyE-tubulin can be observed in WT iNeurons (Figure S6G,H). While polyE tubulin levels seem to increase in WT iNeurons upon AβO exposure, levels are decreasing in tau KO iNeurons. In contrast, re-expression of 0N3R or 1N4R restored the polyE-tubulin levels to WT levels upon AβO exposure, suggesting a restoration of WT-like MT dynamics in these neurons, but with overall little effect.

All in all, our results indicate that the 1N4R tau isoform is sufficient to restore the vulnerability of tau KO iNeurons to AβO-induced reduction of neuronal activity that is observed in WT iNeurons, and that the selective toxicity of 1N4R (in paradigms of disease) is likely based on the significantly higher basal phosphorylation levels within the MT-binding domain at the KxGS motifs.

4 | DISCUSSION

In this study, we describe the successful generation of *MAPT* KO (tau KO) hiPSCs, their differentiation into cortical neurons (iNeurons), basic characterization, introduction of the human brain-specific tau isoforms, and the susceptibility of tau KO iNeurons to AD-like stress via AβO exposure. Tau KO led to mild but detectable alterations of neurite growth and AIS formation. One week post-differentiation, tau KO iNeurons exhibited significant reduction ($\approx$ 30%) in neurite outgrowth, a difference also observed in primary and iPSC-derived cultures of tau-depleted neurons previously,[1,3,7,65] possibly due to the later neuronal fating of our iNeurons compared to primary neurons. At later stages (d18), tau depletion reduced AIS length in line with previous observations.[10] Nonetheless, tau KO did not result in significant changes in neuronal activity, assayed by MEA and spontaneous calcium oscillations. While the mild phenotypes in our iNeurons are in line with previous studies on tau-deficient mice and -derived primary cultures,[1] we could not detect compensatory upregulation of MT-associated proteins (MAP), for example, MAP1A or MAP1B,[2,4] but observed an increased expression of the MAP2 isoform MAP2c, suggesting that a shift in MAP isoform expression and a combination of MAPs rather than upregulation of specific proteins might act as compensatory mechanism for tau loss in human neurons. To confirm that the observed effects on neurite and AIS development were directly linked to tau-KO, we (re-)expressed individual tau isoforms using lentivirus-based delivery. The tau isoforms generally restored neurite and AIS length to WT levels, with 4R tau being more efficient than 3R tau isoforms. All six isoforms restored AIS and neurite length to WT levels individually, indicating that these effects were directly associated with tau loss, and that regulation of neurite extension and AIS length may be essential functions of tau mediated by all isoforms. The presence of six isoforms in the adult brain could, therefore, partially compensate for changes in isoform expression and take over essential tau functions.[24,66,23] Differences in axonal enrichment and intracellular localization have been observed for overexpressed tau isoforms in primary rodent neurons, with larger isoforms like 2N4R, 1N4R, and 2N3R being partially retained in the soma and less efficiently sorted into the axon compared to shorter isoforms like 0N3R.[27–29] This pattern is also present in tau KO iNeurons expressing individual tau isoforms. WT human iNeurons primarily express the shortest tau isoforms (0N3R and 0N4R), which are efficiently sorted into the axon. While all expressed tau isoforms are found in the axons of tau KO iNeurons, none achieved the same sorting efficiency as endogenous tau. Notably, we previously showed that the amount of (over-)expression does not impact sorting efficiency, indicating that with our expression systems the tau sorting machinery is robust,[27,28,67] and because we also found

$N = 4$, $n > 1500$. Statistical significance: $^{*}P \leq 0.05$, $^{**}P \leq 0.01$, $^{***}P \leq 0.001$, ns, not significant. D, Exemplary traces of Fluo-4 signal intensity over 1 minute of tau KO iNeurons expressing either GFP or 1N4R tau after treatment with 1 µM AβOs for 1 hour, indicating spontaneous calcium oscillations and no differences in peak frequency or height between genotypes and treatments. E, Calcium peak count per minute was quantified for tau KO iNeurons transduced with GFP or 1N4R tau after treatment with AβOs for 1 hour using an automated workflow. Error bars represent SEM. Shapiro–Wilk test was performed to test for normal distribution; afterward, statistical analysis was performed by two-way ANOVA with correction for multiple comparisons (Tukey test). $N = 3–4$, $n > 1500$. Ns, not significant. F, Calcium peak height was quantified using an automated workflow after 1 hour treatment with AβOs of tau KO iNeurons expressing either GFP or 1N4R tau. Error bars represent SEM. Shapiro–Wilk test was performed to test for normal distribution; afterward, statistical analysis was performed by two-way ANOVA with correction for multiple comparisons (Tukey test). $N = 3–4$, $n > 1500$. Ns, not significant. G, Quantification of p-tau S262 levels in WT and tau-KO iNeurons transduced with HA-tagged tau isoforms. Error bars represent SEM. Shapiro–Wilk test was performed to test for normal distribution; afterward, statistical analysis was performed by one-way ANOVA with correction for multiple comparisons (Tukey test). $N = 3–4$, $n = 20$. Statistical significance: $^{***}P \leq 0.001$, ns, not significant. H, Representative immunofluorescent images of WT and tau KO iNeurons transduced with $1N4R^{HA}$ or $0N3R^{HA}$ tau isoforms and stained for phosphorylated tau at S262. AβO, amyloid beta oligomer; ANOVA, analysis of variance; KO, knockout; SEM, standard error of the mean; WT, wild type

no differences in turnover, we conclude that other sorting mechanisms must account for the differential sorting. A strong overall correlation between isoform size and axonal enrichment supports findings from primary neurons and rodent brains,[26–29] indicating that higher molecular weight isoforms (2N4R, 2N3R, and 1N4R) are partially retained in the somatodendritic compartment of human neurons, consistent with the AIS-based size-dependent protein filter function with a cut-off ≈ 70 kDa,[68] although 1N4R shows stronger somatic retention compared to its 0N/2N counterparts. PTMs, such as acetylation and phosphorylation, which affect tau's molecular weight and MT-binding affinity, also contribute to axonal sorting efficiency.[1] Indeed, we found that 2N4R and 1N4R tau isoforms are phosphorylated at S262 under basal conditions, suggesting reduced MT binding and lower axonal sorting efficiency. The observed isoform-specific effects of tau on neurite and AIS development could be explained by the differences in the intracellular localization of tau isoforms, and further depend on isoform-specific interactions. Previous studies have demonstrated that murine tau isoforms exhibit a markedly distinct interactome,[69,70] which may also be observed in human tau isoforms. This differential interactome may contribute to the varying efficacies of individual tau isoforms in rescuing the observed growth defects.

Pathological missorting of tau and reduction of neuronal activity can be observed in primary rodent neurons upon treatment with AβOs.[9,45,71] Pathological mis-sorting of tau and reduced neuronal activity measured by calcium oscillations were observed shortly after AβO exposure in our neurons, which was abolished after sustained exposure. Bulk RNAseq analysis of WT iNeurons revealed that nearly all transcriptomic changes were reversed to basal levels after sustained (24-hour) AβO exposure. These findings support that AβOs become less toxic over time due to the formation of larger aggregates.[9] Gene set enrichment analysis identified AβO-affected pathways previously associated with AβO-induced processes, including synapse maintenance, calcium signaling, stress responses, and cell adhesion.[72–76] Consequently, our findings indicate that our human induced neurons are an appropriate model for investigating the pathological mechanisms of AD.

In AD animal models, tau KO protects against APP/AβO-induced pathology.[1,3] Remarkably, we observe the same protective effect of tau KO on AβO-mediated neuronal dysfunction in our human neuronal cultures, which showed no detectable alterations in spontaneous calcium oscillations upon AβO treatment. Calcium oscillations are a powerful proxy for neuronal activity, despite being only an indirect measure of neuronal activity,[77] and in our hands were superior to MEA-based analysis. While associated with slight initial changes in neuronal morphology, tau/*MAPT*-KO (like *Mapt*-KO in murine AD models and -derived neurons) protects from AD-like stress and AβO-mediated suppression of calcium oscillations in our human iNeurons, demonstrating that tau suppression is a relevant target for AD therapy. Upon AβO exposure, tau KO iNeurons expressing 0N4R, 2N4R, or one of the 3R tau isoforms showed a mild reduction of calcium oscillations, indicating partial protection from the observed AβO-induced impairment of neuronal activity. Only the presence of 1N4R tau reduced spontaneous calcium oscillations, indicating impaired neurotransmission and conferred vulnerability of tau-depleted neurons to AβO-mediated suppression of calcium oscillations. These observations suggest that the AβO-induced impairment of calcium oscillations is mediated by 1N4R tau. The effect is, in particular, noteworthy, as a limitation of WT iNeurons is the expression of immature tau isoforms (usually 0N isoforms), as 1N and 2N isoforms are only expressed later in development. Hence, the impactful effect of 1N4R tau on calcium oscillations in response to AβOs is independent of its developmental presence, but might be linked to its presence in the somatodendritic compartment. Tau localization is influenced by several mechanisms, such as PTMs and protein–protein interactions. Our results indicate that 1N4R and 2N4R are significantly higher phosphorylated at S262 than isoforms that are efficiently sorted into the axon. Recently, 2N4R has been shown to re-sensitize primary *Mapt* KO neurons to AβO-induced spine loss, and that knockdown of endogenous 2N4R expression in WT neurons prevented this toxic effect.[29] As both 2N4R and 1N4R are markers of neuronal maturation and are less efficiently sorted into the axon, the mechanism of how these isoforms mediate AβO-induced toxicity might be partially conserved between species. For example, 1N and 2N isoforms show an increased aggregation propensity compared to other isoforms, and the presence of four repeat domains (4R) reduces the critical concentration for fibril formation in vitro.[78,79] Tau further contributes to neuronal dysfunction through a gain-of-toxic function mechanism leading to changed or increased interactions of unbound tau to synaptic components.[80,81] In mice, the interactome of the abundant 2N4R isoform was linked to neurodegenerative processes.[70] In the human brain, 1N tau isoforms are predominantly expressed[24,23] and due to their primarily somatodendritic localization, 1N4R could mediate toxic functions via loss or gain of specific interactions with synaptic proteins, such as Fyn kinase, PSD95, and TTLL6.[80] Further, tau can translocate from dendrites to the post-synapse in an activity-dependent manner, which is disrupted by AβOs, resulting in pathological tau accumulation in dendrites.[82] It has been demonstrated that 1N4R tau oligomers induce a translational stress response, resulting in stress granule formation and changes of dendrite length and morphology that further drive neuronal dysfunction.[1] In combination with that, or alternatively, hyperphosphorylated and mis-sorted tau, accumulating in the soma and dendrites, may scavenge 1N4R tau, inhibiting its dendritic functions. Our findings indicate that 1N4R expression results in a slight increase in polyE-tubulin levels upon AβO exposure. This suggests a potential change in MT dynamics, which may lead to alterations in neuronal function.

The proposed roles of tau under pathological conditions and the observed changes in neuronal activity, somatodendritic localization, and phosphorylation at a pathologically relevant site (S262) in this study provide evidence that somatic and dendritic 1N4R tau is the first mediator of the neurotoxicity observed in human neurons in an AD context. The results indicate that tau-mediated neuronal toxicity is isoform-;specific and likely mediated by dendritic 1N4R, rendering this isoform a promising novel target for the treatment of AD. Our results suggest novel isoform-specific roles of tau in neurite and AIS development, and neuronal activity. In addition, we showed that tau KO confers protection against AD-like stress in human neurons. Our results indi-

cate that 1N4R tau is crucial for tau-mediated neuronal dysfunction and represents a potential therapeutic target for the treatment of AD. Consequently, future studies must consider the differential contributions of tau isoforms to neuronal development and dysfunction in disease paradigms, with a particular focus on the targeting of specific isoforms such as 1N4R to mitigate tau-related pathologies.

AUTHOR CONTRIBUTIONS

Sarah Buchholz: study design, data acquisition, analysis, data interpretation, and manuscript drafting. Michael Bell-Simons, Jennifer Klimek, Mohamed Aghyad Al Kabbani, Marcos R. Costa, Lukas C. Iohan, Natja Haag, Lena Kluge, Cagla Cagmak, Audrey Coulon, and Devrim Kilinc: assistance in data acquisition, analysis, and methodology development. Michael Bell-Simons, Natja Haag, and Marcos R. Costa: manuscript proofreading. Hans Zempel: project funding, providing of concept, study design, interpretation of data, and manuscript drafting. All authors contributed to the article and approved the final manuscript.

ACKNOWLEDGMENTS

We thank Prof. Dr. Li Gan (Weill Cornell Medicine, NY, USA) for providing *Ngn2*-WTC11 iPSCs and Andrea Delle Vedove (Institute of Human Genetics, Cologne, Germany) for help with the ImageJ macro for calcium imaging analysis. We thank Lea Hund (University of Cologne) for supporting the off-target sequencing of tau KO clones. We thank Prof. Dr. Florian Klein (Institute of Virology, University Hospital Cologne) for providing lentiviral vectors. Stem cell work was performed at the iPSC-Lab core facility of the CMMC (Cologne, Germany). Mice were provided by CMMC animal facility and CECAD in vivo research facility (both Cologne, Germany). We thank the CECAD Proteomics Facility for the analysis of proteome data. Our work is supported by the Else-Kröner-Fresenius-Stiftung, the DFG/GRC, Koeln Fortune Program/Faculty of Medicine, University of Cologne (all to H.Z.); a stipend from the Studienstiftung des Deutschen Volkes (to M.B.S.); and the Jürgen-Manchot-Stiftung (to C.C.). This work was supported by the large instrument grant INST 1856/71-1 FUGG by the German Research Foundation (DFG Großgeräteantrag). Partial support for Open Access funding by Project DEAL. We acknowledge support from Alzheimer Forschung Initiative e.V. for Open Access Publishing.

CONFLICT OF INTEREST STATEMENT

The authors declare no conflicts of interest.

ORCID

Sarah Buchholz https://orcid.org/0000-0002-3636-1364
Marcos R. Costa https://orcid.org/0000-0002-4928-2163
Devrim Kilinc https://orcid.org/0000-0003-3321-5203
Hans Zempel https://orcid.org/0000-0002-7510-3077

REFERENCES

1. Buchholz S, Zempel H. The six brain-specific tau isoforms and their role in Alzheimer's disease and related neurodegenerative dementia syndromes. *Alzheimers Dement*. 2024;20: 3606-3628. doi:10.1002/alz.13784
2. Baas PW, Qiang L. Tau: it's not what you think. *Trends Cell Biol*. 2019;29:452-461. doi:10.1016/J.TCB.2019.02.007
3. Ke YD, Suchowerska AK, Van Der Hoven J, et al. Lessons from Tau-deficient mice. *Int J Alzheimers Dis*. 2012. doi:10.1155/2012/873270
4. Dawson HN, Ferreira A, Eyster MV, Ghoshal N, Binder LI, Vitek MP. Inhibition of neuronal maturation in primary hippocampal neurons from tau deficient mice. *J Cell Sci*. 2001;114(Pt 6): 1179-87. doi: 10.1242/jcs.114.6.1179
5. Qiang L, Sun X, Austin TO, et al. Tau does not stabilize axonal microtubules but rather enables them to have long labile domains. *Curr Biol*. 2018;28:2181-2189.e4. doi:10.1016/j.cub.2018.05.045
6. Caceres A, Kosik KS. Inhibition of neurite polarity by tau antisense oligonucleotides in primary cerebellar neurons. *Nature*. 1990;343:461-463. doi:10.1038/343461a0
7. Caceres A, Potrebic S, Kosik KS. The effect of tau antisense oligonucleotides on neurite formation of cultured cerebellar macroneurons. *J Neurosci*. 1991;11:1515-1523. doi:10.1523/JNEUROSCI.11-06-01515.1991
8. Tint I, Slaughter T, Fischer I, Black MM. Acute inactivation of tau has no effect on dynamics of microtubules in growing axons of cultured sympathetic neurons. *J Neurosci*. 1998;18:8660-8673. doi:10.1523/JNEUROSCI.18-21-08660.1998
9. Zempel H, Luedtke J, Kumar Y, et al. Amyloid-β oligomers induce synaptic damage via Tau-dependent microtubule severing by TTLL6 and spastin. *EMBO J*. 2013;32:2920-2937. doi:10.1038/EMBOJ.2013.207
10. Bessone IF, Damianich A, Pedroncini O, et al. Tau conditional reduction in human-derived neurons exposes novel tau-associated functions in electrical activity and axonal transport. *Alzheimers Dement*. 2021;17:e052863. doi:10.1002/ALZ.052863
11. Pontecorvo MJ, Devous MD, Kennedy I, et al. A multicentre longitudinal study of flortaucipir (18F) in normal ageing, mild cognitive impairment and Alzheimer's disease dementia. *Brain*. 2019;142:1723-1735. doi:10.1093/BRAIN/AWZ090
12. Price JL, McKeel DW, Buckles VD, et al. Neuropathology of nondemented aging: presumptive evidence for preclinical Alzheimer disease. *Neurobiol Aging*. 2009;30:1026-1036. doi:10.1016/J.NEUROBIOLAGING.2009.04.002
13. Price JL, Morris JC. Tangles and plaques in nondemented aging and "preclinical" Alzheimer's disease. *Ann Neurol*. 1999;45:358-368. doi:10.1002/1531-8249(199903)45:3<358::AID-ANA12>3.0.CO;2-X
14. Giannakopoulos P, Herrmann FR, Bussière T, et al. Tangle and neuron numbers, but not amyloid load, predict cognitive status in Alzheimer's disease. *Neurology*. 2003;60:1495-1500. doi:10.1212/01.WNL.0000063311.58879.01
15. Nelson PT, Alafuzoff I, Bigio EH, et al. Correlation of Alzheimer disease neuropathologic changes with cognitive status: a review of the literature. *J Neuropathol Exp Neurol*. 2012;71:362-381. doi:10.1097/NEN.0B013E31825018F7
16. Rapoport M, Dawson HN, Binder LI, Vitek MP, Ferreira A. Tau is essential to beta -amyloid-induced neurotoxicity. *Proc Natl Acad Sci U S A*. 2002;99:6364-6369. doi:10.1073/pnas.092136199
17. Roberson ED, Scearce-Levie K, Palop JJ, et al. Reducing endogenous tau ameliorates amyloid beta-induced deficits in an Alzheimer's disease mouse model. *Science*. 2007;316:750-754. doi:10.1126/SCIENCE.1141736
18. Shipton OA, Leitz JR, Dworzak J, et al. Tau protein is required for amyloid {beta}-induced impairment of hippocampal long-term potentiation. *J Neurosci*. 2011;31:1688-1692. doi:10.1523/jneurosci.2610-10.2011
19. DeVos SL, Miller RL, Schoch KM, et al. Tau reduction prevents neuronal loss and reverses pathological tau deposition and seeding in mice with tauopathy. *Sci Transl Med*. 2017;9:eaag0481. doi:10.1126/scitranslmed.aag0481

20. Vossel KA, Zhang K, Brodbeck J, et al. Tau reduction prevents Abeta-induced defects in axonal transport. *Science*. 2010;330. doi:10.1126/SCIENCE.1194653
21. Goedert M, Spillantini MG, Jakes R, Rutherford D, Crowther RA. Multiple isoforms of human microtubule-associated protein tau: sequences and localization in neurofibrillary tangles of Alzheimer's disease. *Neuron*. 1989. doi:10.1016/0896-6273(89)90210-9
22. Andreadis A, Brown WM, Kosik KS. Structure and novel exons of the human.tau.gene. *Biochemistry*. 1992;31:10626-10633. doi:10.1021/bi00158a027
23. Trabzuni D, Wray S, Vandrovcova J, et al. MAPT expression and splicing is differentially regulated by brain region: relation to genotype and implication for tauopathies. *Hum Mol Genet*. 2012;21:4094-4103. doi:10.1093/HMG/DDS238
24. Bullmann T, Holzer M, Mori H, Arendt T. Pattern of tau isoforms expression during development in vivo. *Int J Dev Neurosci*. 2009;27:591-597. doi:10.1016/J.IJDEVNEU.2009.06.001
25. Bullmann T, de Silva R, Holzer M, Mori H, Arendt T. Expression of embryonic tau protein isoforms persist during adult neurogenesis in the hippocampus. *Hippocampus*. 2007;17:98-102. doi:10.1002/hipo.20255
26. Liu C, Götz J. Profiling murine tau with 0N, 1N and 2N isoform-specific antibodies in brain and peripheral organs reveals distinct subcellular localization, with the 1N Isoform being enriched in the nucleus. *PLoS One*. 2014;8:e84849. doi:10.1371/journal.pone.0084849
27. Zempel H, Dennissen FJA, Kumar Y, et al. Axodendritic sorting and pathological missorting of Tau are isoform-specific and determined by axon initial segment architecture. *J Biol Chem*. 2017;292:12192-12207. doi:10.1074/jbc.M117.784702
28. Bachmann S, Bell M, Klimek J, Zempel H. Differential effects of the six human tau isoforms: somatic retention of 2N-tau and increased microtubule number induced by 4R-tau. *Frontiers in Neuroscience*. 2021;15:547.
29. Buchholz S, Zempel H. Suppression of mature tau isoforms prevents Alzheimer's disease-like amyloid-beta oligomer-induced spine loss in rodent neurons. *Neural Regen Res*. 2023;19(8):1655-1657. doi:10.4103/1673-5374.389644 https://accepted/manuscript
30. Langerscheidt F, Wied T, Al Kabbani MA, van Eimeren T, Wunderlich G, Zempel H. Genetic forms of tauopathies: inherited causes and implications of Alzheimer's disease-like tau pathology in primary and secondary tauopathies. *J Neurol*. 2024;2024:1-27. doi:10.1007/S00415-024-12314-3
31. Drummond E, Wisniewski T. Alzheimer's disease: experimental models and reality. *Acta Neuropathologica*. 2016;133(2):155-175. doi:10.1007/S00401-016-1662-X
32. Miyaoka Y, Chan AH, Judge LM, et al. Isolation of single-base genome-edited human iPS cells without antibiotic selection. *Nat Methods*. 2014;11:291-293. doi:10.1038/nmeth.2840
33. Wang C, Ward ME, Chen R, et al. Scalable production of iPSC-derived human neurons to identify tau-lowering compounds by high -content screening. *Stem Cell Rep*. 2017;9. doi:10.1016/j.stemcr.2017.08.019
34. Buchholz S, Bell-Simons M, Cakmak C, Klimek J, Gan L, Zempel H. Cultivation, differentiation, and lentiviral transduction of human-induced pluripotent stem cell (hiPSC)-derived glutamatergic neurons for studying human tau. *Methods Mol Biol*. 2024;2754:533-549. doi:10.1007/978-1-0716-3629-9_31/FIGURES/2
35. Bachmann S, Linde J, Bell M, Spehr M, Zempel H, Zimmer-Bensch G. DNA methyltransferase 1 (DNMT1) shapes neuronal activity of human iPSC-derived glutamatergic cortical neurons. *Int J Mol Sci*. 2021;22. doi:10.3390/ijms22042034
36. Buchholz S, Bell-Simons M, Cakmak C, Klimek J, Gan L, Zempel H. Cultivation, differentiation, and lentiviral transduction of Human-Induced Pluripotent Stem Cell (hiPSC)-derived glutamatergic neurons for studying human Tau. In: Smet-Nocca, C, ed. *Tau Protein: Methods in Molecular Biology*, Vol 2754. Humana; 2024; 533-549. doi:https://doi.org/10.1007/978-1-0716-3629-9_31
37. Adachi K, Kopp W, Wu G, et al. Esrrb unlocks silenced enhancers for reprogramming to naive pluripotency. *Cell Stem Cell*. 2018;23:266-275.e6. doi:10.1016/J.STEM.2018.05.020
38. Demichev V, Messner CB, Vernardis SI, Lilley KS, Ralser M. DIA-NN: neural networks and interference correction enable deep proteome coverage in high throughput. *Nat Methods*. 2019;17:41-44. doi:10.1038/s41592-019-0638-x
39. Tyanova S, Temu T, Sinitcyn P, et al. The Perseus computational platform for comprehensive analysis of (prote)omics data. *Nat Methods*. 2016;13:731-740. doi:10.1038/NMETH.3901
40. Zempel H, Mandelkow EM. Tracking Tau in neurons: how to grow, fix, and stain primary neurons for the investigation of Tau in all developmental stages. *Methods in Mol Biol*. 2017; 1523. doi:10.1007/978-1-4939-6598-4_20
41. Buchholz S, Bell-Simons M, Haag N, Zempel H. Tracking Tau in neurons: how to grow, fix, and stain primary neurons for the investigation of Tau in all developmental stages. In: Smet-Nocca, C, ed. *Tau Protein: Methods in Molecular Biology*. Vol 2754. Humana; 2024:507-519. doi:10.1007/978-1-0716-3629-9_29
42. Meijering E, Jacob M, Sarria JCF, Steiner P, Hirling H, Unser M. Design and validation of a tool for neurite tracing and analysis in fluorescence microscopy images. *Cytometry Part A*. 2004;58A:167-176. doi:10.1002/CYTO.A.20022
43. Lou E, Fujisawa S, Morozov A, et al. Tunneling nanotubes provide a unique conduit for intercellular transfer of cellular contents in human malignant pleural mesothelioma. *PLoS One*. 2012;7:e33093. doi:10.1371/JOURNAL.PONE.0033093
44. Dull T, Zufferey R, Kelly M, et al. A third-generation lentivirus vector with a conditional packaging system. *J Virol*. 1998;72:8463-8471. doi:10.1128/JVI.72.11.8463-8471.1998
45. Schützmann MP, Hasecke F, Bachmann S, et al. Endo-lysosomal Aβ concentration and pH trigger formation of Aβ oligomers that potently induce Tau missorting. *Nat Commun*. 2021;12:1-14. doi:10.1038/s41467-021-24900-4
46. Bray NL, Pimentel H, Melsted P, Pachter L. Near-optimal probabilistic RNA-seq quantification. *Nat Biotechnol*. 2016;34:525-527. doi:10.1038/nbt.3519
47. Soneson C, Love MI, Robinson MD. Differential analyses for RNA-seq: transcript-level estimates improve gene-level inferences. *F1000Research*. 2016;4:1521. doi:10.12688/f1000research.7563.2
48. Love MI, Huber W, Anders S. Moderated estimation of fold change and dispersion for RNA-seq data with DESeq2. *Genome Biol*. 2014;15:1-21. doi:10.1186/S13059-014-0550-8/FIGURES/9
49. Korotkevich G, Sukhov V, Budin N, Shpak B, Artyomov MN, Sergushichev A. Fast gene set enrichment analysis. *BioRxiv*. 2021:060012. doi:10.1101/060012
50. Vitting-Seerup K, Sandelin A. The landscape of isoform switches in human cancers. *Mol Cancer Res*. 2017;15:1206-1220. doi:10.1158/1541-7786.MCR-16-0459/14585/AM/THE-LANDSCAPE-OF-ISOFORM-SWITCHES-IN-HUMAN
51. Reyes A, Anders S, Weatheritt RJ, Gibson TJ, Steinmetz LM, Huber W. Drift and conservation of differential exon usage across tissues in primate species. *Proc Natl Acad Sci U S A*. 2013;110:15377-15382. doi:10.1073/PNAS.1307202110/SUPPL_FILE/SD01.PDF
52. Kang YJ, Yang DC, Kong L, Hou M, Meng YQ, Wei L, et al. CPC2: a fast and accurate coding potential calculator based on sequence intrinsic features. *Nucleic Acids Res*. 2017;45:W12-W16. doi:10.1093/NAR/GKX428
53. Punta M, Coggill PC, Eberhardt RY, et al. The Pfam protein families database. *Nucleic Acids Res*. 2012;40:D290-D301. doi:10.1093/NAR/GKR1065

54. Almagro Armenteros JJ, Tsirigos KD, Sønderby CK, et al. SignalP 5.0 improves signal peptide predictions using deep neural networks. *Nat Biotechnol*. 2019;37:420-423. doi:10.1038/s41587-019-0036-z
55. Klausen MS, Jespersen MC, Nielsen H, et al. NetSurfP-2.0: improved prediction of protein structural features by integrated deep learning. *Proteins*. 2019;87:520-527. doi:10.1002/PROT.25674
56. Bell M, Bachmann S, Klimek J, Langerscheidt F, Zempel H. Axonal tau sorting requires the C-terminus of tau but is independent of ANKG and TRIM46 enrichment at the AIS. *Neuroscience*. 2021;461:155-171. doi:10.1016/J.NEUROSCIENCE.2021.01.041
57. Schwarz JM, Cooper DN, Schuelke M, Seelow D. MutationTaster2: mutation prediction for the deep-sequencing age. *Nat Methods*. 2014;11:361-362. doi:10.1038/nmeth.2890
58. Johnson MA, Weick JP, Pearce RA, Zhang SC. Functional neural development from human embryonic stem cells: accelerated synaptic activity via astrocyte coculture. *J Neurosci*. 2007;27:3069-3077. doi:10.1523/JNEUROSCI.4562-06.2007
59. Balaji V, Kaniyappan S, Mandelkow E, Wang Y, Mandelkow EM. Pathological missorting of endogenous MAPT/Tau in neurons caused by failure of protein degradation systems. *Autophagy*. 2018; 14(12), 2139-2154. doi:10.1080/15548627.2018.1509607
60. Ittner LM, Ke YD, Delerue F, et al. Dendritic function of tau mediates amyloid-beta toxicity in Alzheimer's disease mouse models. *Cell*. 2010;142:387-397. doi:10.1016/j.cell.2010.06.036
61. Kuperstein I, Broersen K, Benilova I, et al. Neurotoxicity of Alzheimer's disease Aβ peptides is induced by small changes in the Aβ42 to Aβ40 ratio. *EMBO J*. 2010;29:3408-3420. doi:10.1038/EMBOJ.2010.211
62. Knopman DS, Amieva H, Petersen RC, et al. Alzheimer disease. *Nat Rev Dis Primers*. 2021;7:33. doi:10.1038/s41572-021-00269-y
63. Xu Z, Schaedel L, Portran D, et al. Microtubules acquire resistance from mechanical breakage through intralumenal acetylation. *Science (1979)*. 2017;356:328-332. doi:10.1126/SCIENCE.AAI8764/SUPPL_FILE/MOVIES_S5-S10.ZIP
64. Bodakuntla S, Janke C, Magiera MM. Tubulin polyglutamylation, a regulator of microtubule functions, can cause neurodegeneration. *Neurosci Lett*. 2021;746:135656. doi:10.1016/J.NEULET.2021.135656
65. Ng B, Vowles J, Bertherat F, et al. Tau depletion in human neurons mitigates Aβ-driven toxicity. *Mol Psychiatry*. 2024:1-12. doi:10.1038/s41380-024-02463-2
66. Goedert M, Spillantini MG, Potier MC, Ulrich J, Crowther RA. Cloning and sequencing of the cDNA encoding an isoform of microtubule-associated protein tau containing four tandem repeats: differential expression of tau protein mRNAs in human brain. *EMBO J*. 1989;8:393. doi:10.1002/j.1460-2075.1989.tb03390.x
67. Bell-Simons M, Buchholz S, Klimek J, Zempel H. Axonal Tau sorting depends on the PRR2 domain and 0N4R-specific interactions hint at distinct roles of Tau isoforms in synaptic plasticity. *BioRxiv*. 2024;2024. doi:10.1101/2024.06.28.601286
68. Li X, Kumar Y, Zempel H, Mandelkow E, Biernat J, Mandelkow E. Novel diffusion barrier for axonal retention of Tau in neurons and its failure in neurodegeneration. *EMBO J*. 2011;30:4825-4837. doi:10.1038/emboj.2011.376
69. Tracy TE, Madero-Pérez J, Swaney DL, et al. Tau interactome maps synaptic and mitochondrial processes associated with neurodegeneration. *Cell*. 2022;185:712-728.e14. doi:10.1016/J.CELL.2021.12.041/ATTACHMENT/418D38D8-6F98-4567-AE33-02B961DF13F7/MMC6.XLSX
70. Liu C, Song X, Nisbet R, Götz J. Co-immunoprecipitation with Tau isoform-specific antibodies reveals distinct protein interactions and highlights a putative role for 2N tau in disease. *J Biol Chem*. 2016;291:8173-8188. doi:10.1074/JBC.M115.641902
71. Zempel H, Thies E, Mandelkow E, Mandelkow EM. Abeta oligomers cause localized Ca(2+) elevation, missorting of endogenous Tau into dendrites, Tau phosphorylation, and destruction of microtubules and spines. *J Neurosci*. 2010;30:11938-11950. doi:10.1523/JNEUROSCI.2357-10.2010
72. Tong BCK, Wu AJ, Li M, Cheung KH. Calcium signaling in Alzheimer's disease & therapies. *Biochim Biophys Acta Mol Cell Res*. 2018;1865:1745-1760. doi:10.1016/J.BBAMCR.2018.07.018
73. Lazzari C, Kipanyula MJ, Agostini M, Pozzan T, Fasolato C. Aβ42 oligomers selectively disrupt neuronal calcium release. *Neurobiol Aging*. 2015;36:877-885. doi:10.1016/J.NEUROBIOLAGING.2014.10.020
74. Meftah S, Gan J. Alzheimer's disease as a synaptopathy: evidence for dysfunction of synapses during disease progression. *Front Synaptic Neurosci*. 2023;15:1129036. doi:10.3389/FNSYN.2023.1129036/BIBTEX
75. Pfundstein G, Nikonenko AG, Sytnyk V. Amyloid precursor protein (APP) and amyloid β (Aβ) interact with cell adhesion molecules: implications in Alzheimer's disease and normal physiology. *Front Cell Dev Biol*. 2022;10:969547. doi:10.3389/FCELL.2022.969547/BIBTEX
76. Uddin MS, Yu WS, Lim LW. Exploring ER stress response in cellular aging and neuroinflammation in Alzheimer's disease. *Ageing Res Rev*. 2021;70:101417. doi:10.1016/J.ARR.2021.101417
77. Ali F, Kwan AC. Interpreting in vivo calcium signals from neuronal cell bodies, axons, and dendrites: a review. *Neurophotonics*. 2019;7:011402. doi:10.1117/1.NPH.7.1.011402
78. Goedert M, Jakes R. Expression of separate isoforms of human tau protein: correlation with the tau pattern in brain and effects on tubulin polymerization. *EMBO J*. 1990;9:4225-4230.
79. Zhong Q, Congdon EE, Nagaraja HN, Kuret J. Tau isoform composition influences rate and extent of filament formation. *J Biol Chem*. 2012;287:20711-20719. doi:10.1074/JBC.M112.364067
80. Ittner A, Ittner LM. Dendritic tau in Alzheimer's Disease. *Neuron*. 2018;99:13-27. doi:10.1016/J.NEURON.2018.06.003
81. Zempel H, Mandelkow E. Lost after translation: missorting of Tau protein and consequences for Alzheimer disease. *Trends Neurosci*. 2014;37:721-732. doi:10.1016/J.TINS.2014.08.004
82. Frandemiche ML, De Seranno S, Rush T, et al. Activity-dependent tau protein translocation to excitatory synapse is disrupted by exposure to amyloid-beta oligomers. *J Neurosci*. 2014;34:6084-6097. doi:10.1523/jneurosci.4261-13.2014

SUPPORTING INFORMATION

Additional supporting information can be found online in the Supporting Information section at the end of this article.

How to cite this article: Buchholz S, Kabbani M, Bell-Simons M, et al. The tau isoform 1N4R confers vulnerability of *MAPT* knockout human iPSC-derived neurons to amyloid beta and phosphorylated tau-induced neuronal dysfunction. *Alzheimer's Dement*. 2025;21:e14403. https://doi.org/10.1002/alz.14403